Manuscript 6130, Revision 1
Submission to the Special Collection: Mechanisms, Rates, and Timescales of Geochemical Transport in the Crust and Mantle

Element mobility during regional metamorphism in crustal and subduction zone environments with a focus on the rare earth elements (REE)

Jay J. Ague[1,2]

[1]Department of Geology and Geophysics
Yale University
P.O. Box 208109
New Haven, CT 06520-8109 USA
jay.ague@yale.edu

[2]Peabody Museum of Natural History
Yale University
New Haven, CT 06511 USA

Abstract

This paper explores bulk-rock geochemical data for a wide array of metamorphosed mafic, quartzofeldspathic, pelitic, and metacarbonate rocks using a quantitative mass balance approach to assess fluid-driven element mobility—particularly of the rare earth elements (REE)—in regional metamorphic and some high pressure subduction zone environments (40 examples; over 240 individual analyses). The results highlight the critical role of mineral reactions in controlling rock compositions and compositional changes. Most examples are from focused fluid flow settings, such as veins and lithologic contacts, where fluxes are large and metasomatic signals are thus strong. A variety of REE behaviors are observed, including little or no REE mobility (roughly 1/3 of the data set); light REE (LREE), mid-REE (MREE), and/or heavy (HREE) mobility; europium "anomalies"; overall REE losses; and local REE redistribution. The REE are typically fractionated by mass transfer, with the exception of several examples that underwent fairly uniform overall losses of REE. The fractionation reflects strong mineralogical controls on REE uptake/loss by rocks by a comparatively small number of phases. Examples include: HREE mass changes associated with garnet, xenotime, and sphene; LREE and MREE changes associated with apatite, monazite, and allanite; and Eu changes associated with plagioclase and lawsonite. As mineralogy is a dominant control, the nature of the metasomatism is not strongly correlated with metamorphic grade, other than obvious mineralogical differences between settings (e.g., plagioclase in Barrovian metamorphism, lawsonite in subduction zones). Extensive mobilization of non-REE major and trace elements can happen without significant open-system transport of the REE. If REE mobility occurs, it is always accompanied by mobilization of other non-REE. When mobile, neighboring REE (e.g., Sm and Nd) typically have strongly correlated mass changes indicating that both were mobilized

to about the same degree. Thus, constancy of neighboring REE mass ratios does not mean that they were immobile. Although individual examples of metasomatism can show correlations between patterns of mass transfer for the REE and the non-REE, little such correlation is evident across the entire data set, with the exception of P. Once again, this highlights the importance of individual minerals in controlling REE systematics. REE mass transfer coupled to gains or losses of volatiles is also not evident, although more data are clearly needed to document the impact of F, Cl, CO_2, sulfur, and other species on REE behavior. Broad correlations of REE and P mobility suggest REE transport by P complexes, or REE and P transport together by some other complexing agent. Mass changes for REE and Y are more strongly coupled, reflecting the geochemical similarity of these elements and perhaps indicating a role for Y complexing as well.

The REE are the most mobile of the high-field strength elements (HFSE). On a percentage mass basis the amount of HFSE mobility decreases roughly in the order: REE>U>Nb>Ti>Th~Zr. Th mobility is rare but when present is positively correlated with U and REE mobility. The mobility of the more refractory HFSE is low in aqueous fluids, but is a larger concern in more extreme environments such as magmatic/magmatic-hydrothermal systems, charnockite metamorphism, and supercritical fluids in high-pressure/ultrahigh-pressure settings. The mobility of certain HFSE (e.g., Nb) can be large enough to affect rock plotting positions on petrotectonic discrimination diagrams.

Potassium and related (Rb, Ba, Cs) large-ion lithophile elements (LILE) are typically lost in association with mica breakdown. As the data set focuses on high fluid flow environments, LILE changes will likely be smaller for rocks that undergo less fluid-rock interaction. Gains of K and related LILE are coupled to volatile gain and Na loss, consistent with fluid flow down temperature gradients, or infiltration from K-rich sources (e.g., pegmatites). In Barrovian

settings, two other mass transfer trends are evident in addition to K mass transfer. First, silica loss is coupled to volatile loss, illustrating the dependence of silica mass transfer on devolatilization. Most of the silica loss reflects local mass transfer into adjacent vein fluid flow conduits were additional silica is precipitated; indeed, wallrock inclusions in veins can be highly silicified. Second, Na and Ca mass gains and losses are well correlated in the Barrovian examples, reflecting control of plagioclase growth or destruction. Strontium and Pb behaviors also appear to be largely related to plagioclase behavior (in subduction settings, this role can be played by phases such as lawsonite or epidote group minerals).

Carbon dioxide mass transfer by conventional devolatilization as well as near-stoichiometric $CaCO_3$ dissolution or precipitation are represented in the data set. Determining the relative roles of these processes as functions of metamorphic grade, intensity of fluid-rock interaction, and tectonic setting will be an important challenge for future research.

Introduction

Time-integrated fluid fluxes due to crustal devolatilization during regional metamorphism of sedimentary rock-dominated sequences can attain ~10^3 m^3 m^{-2} averaged over regional scales (e.g., Wickham and Tayor, 1985; Ague, 1994b, 2014; Ferry, 1994; Skelton et al., 1996; Bickle, 1996; Hanson, 1997; Lyubetskaya and Ague, 2009). In other words, a column of fluid ~1 km long passes through a 1 m^2 area of rock oriented perpendicular to flow. Fluxes of this magnitude will be an unavoidable consequence of prograde fluid generation in such sequences. Fluxes upward through subducted oceanic crust are also large and have been estimated to be ~300 m^3 m^{-2} (Zack and John, 2007), but could be even larger depending on the hydration state of subducted mantle (e.g., Faccenda et al. 2009) or if focused along the slab-mantle wedge interface (e.g., Wilson et al. 2014).

These fluxes transfer massive quantities of H_2O, CO_2, CH_4, and other volatile species from actively metamorphosing regions in the lithosphere to the shallow crust and hydrosphere. In so doing, they drive reaction progress (particularly in carbonate-bearing rocks), exert strong controls on rock rheology and deformation behavior, determine the onset of partial melting in the crust and mantle wedge and, ultimately, influence the long-term global carbon cycle.

Such fluxes are undeniably large, but whether or not they can regionally transport "non-volatile" elements such as the alkalis, alkaline earths, transition metals, and rare earth elements (REE) depends strongly on the nature of flow. If the flow is everywhere uniform and pervasive at the grain scale, then maximum fluxes in any given part of the rock mass are limited to values in the 10^3 m^3 m^{-2} range. On the other hand, if the flow is focused into some form of conduit, then within conduits fluxes can be far larger than regional average values by one or even two orders of magnitude (Fig. 1). Of course, this also means that areas outside of a conduit are impoverished

in fluid, because fluid is diverted away from them. It is in the more focused flow regimes that non-volatile element transfer on large scales will occur most readily, at time-integrated fluxes of ~10^4 to ~10^6 m^3 m^{-2}.

Focusing generally results from rock permeability variations. High-permeability areas will have the best potential to evolve into fluid conduits. Examples are many, and include high-permeability layers, fractures and veins, boudin necks, shear zones, mélange zones, high permeability regions developed in certain compacting two-phase flow systems (Connolly and Podladchikov, 2007), fold hinges (e.g., Skelton et al. 1995), and lithologic contacts (for reviews see, e.g., Oliver, 1996; Ague, 2014). It is straightforward to illustrate how increasing the permeability and proportions of conduits can drastically alter the hydrologic regime. Consider unidirectional flow where 10 volume percent of the rock mass is composed of conduits parallel to the flow direction that are a factor of 10^2 more permeable than the surroundings. From Darcy's law, more than 90% of the total fluid flow is carried by the conduits (assuming uniform fluid pressure gradient and viscosity across the flow region). Permeability variations of this magnitude are easily conceivable; for example, for planar cracks, permeability scales as the cube of the crack aperture (e.g., Norton and Knapp, 1977).

The aim of this paper is to examine chemical changes in rocks brought on by focused fluid flow in the continental crust and in subduction zones (mostly <~2.5 GPa) up to, but not including, the realm of extensive partial melting. There are many chemical elements to consider—too many for one paper—so the main theme will be mobility of the rare earth elements (REE). Other elements such as large-ion lithophile (LILE) and high-field strength (HFSE) elements will be discussed when appropriate.

Historically, REE mobility has commonly been inferred to be relatively limited during hydrothermal or metamorphic fluid-rock interaction, and this is indeed the case in many environments (e.g., Taylor and McLennan, 1985; Michard and Albarède, 1986; Banner and Hanson, 1990; Bau, 1991). Nonetheless, clear examples of transport have been well documented. REE transport in fluids has broad implications for understanding the nature and timing of a wide array of lithospheric processes. For example, determining the tectonic setting of magmatism using trace element discrimination diagrams is predicated on little or no REE mobility subsequent to igneous crystallization (e.g., Pearce et al. 1984). Dating of garnet growth events using Sm-Nd or Lu-Hf isotope systematics likewise requires REE immobility in the host rock (e.g., Baxter and Scherer, 2013). Mobility must also be carefully assessed when interpreting whole-rock isochrons (e.g., O'Neill et al. 2012). REE mobility during subduction, or lack thereof, exerts important controls on arc magma chemistry as well as the REE budget of lithosphere subducted deep into Earth's mantle beyond the arc magma window (e.g., Sorensen and Grossman, 1989; Spandler et al. 2003; 2004; Zack and John, 2007; Miller et al. 2009; Bebout, 2014; Bebout and Penniston-Dorland, 2016; Taetz et al. 2016).

A wide range of approaches have been applied to assess REE mobility. A common strategy is to compare the chondrite-normalized REE patterns of a suite of low-grade protoliths to those of higher-grade rocks. This approach has been used, for example, to deduce little REE mobility in subduction complex rocks from western Liguria (Tribuzio et al. 1996) and New Caledonia (Spandler et al. 2003; 2004). Variability of REE patterns can also provide clues to transport. Zhao et al. (2007) found that light REE (LREE) patterns in UHP eclogites from the Sulu orogen ranged widely, whereas HREE patterns were more or less constant. They concluded that the LREE variability resulted from mobilization, but that the HREE were immobile. Similar

147 conclusions regarding larger LREE mobility relative to heavier REE have been reached in a
148 variety of other studies (e.g., Weaver and Tarney, 1981; Griffin and Brueckner, 1985; Zack and
149 John, 2007). The presence of isotopic disequilibrium, as evidenced by, for example, negative
150 Sm-Nd model ages, or extreme ranges of Nd isotopic ratios, are further indicators of REE
151 transport (e.g., Windrim et al. 1984; Munz et al. 1994).

152 This paper will center on selected studies for which the mass balance assessment of
153 element transport, including major and trace elements, is feasible. This is related to, but distinct
154 from, the ever-growing body of work that has illuminated REE partitioning between phases at
155 the scale of hand samples or thin sections. Such REE redistribution can be the result of
156 progressive reaction in closed or nearly closed systems, and need not indicate mobility into or
157 out of a rock mass. Studies of the REE patterns of individual phases are a critical aspect of
158 understanding the geochemistry of REE, but our focus is mostly on bulk-rock chemistry and the
159 prospect of larger-scale mobility in focused flow environments including veins, lithologic
160 contacts, and shear zones. REE mobility in shallow and/or low-temperature settings including
161 hydrothermal seafloor alteration, burial metamorphism, and contact metamorphic phenomena
162 such as skarns (e.g., Hellman et al. 1979; Windrim et al. 1984; Bartley, 1986; Gruau et al. 1992;
163 Marsh et al. 2012; Durand et al, 2015; Floess et al. 2015) is for the most part not considered, the
164 emphasis being placed on deeper lithospheric processes.

165 Most of the data has been published; some is presented here for the first time (Table 1).
166 The data set is by no means exhaustive, but it nonetheless attempts to document the more
167 common sorts of mobility recognized in nature.

168 **Some Comments on Determining Chemical Changes in Rocks**

Mass balance analysis compares rocks that have been chemically changed by fluid infiltration to those that have not in order to determine what elements have been gained or lost. The governing equations describing mass and volume changes have been well studied; derivations and discussion can be found in, for example, Gresens (1967), Grant (1986), Brimhall and Dietrich (1987), Brimhall et al. (1988), Ague (1994a), and Baumgartner and Olsen (1995). A brief summary is given in the appendix. The final mass balance expressions are similar regardless of treatment, although Brimhall and Dietrich (1987) and Brimhall et al. (1988) illuminated the relationships between mass change, rock and mineral density, porosity, and volume change.

Closure

Despite the straightforward mathematical nature of the equations, the basic problem of how to quantify rock mass and volume changes has generated a remarkable amount of confusion over the years. The source of much of this confusion is the fact that increases or decreases in the weight percent or ppm of an element need not correlate with actual gains or losses of the mass of that element. At first, this seems very counterintuitive. If the concentration of, for example, La increases from 100 to 125 ppm during some fluid-driven mass transfer event, doesn't that have to mean that the rock gained La?

It turns out that there is more than one explanation and La need not have been gained. Suppose that 20 wt. % silica was removed from the rock due to, for example, local diffusion to an adjacent quartz vein. Such mass changes are commonly observed (e.g., Ague, 1994b; Penniston-Dorland and Ferry, 2008). So 100 g of rock now has a mass of 80 g. Let us further assume that La was immobile during this alteration. Compositions are normalized to 100 wt. %, so the new La concentration is: (100 ppm/80) 100 = 125 ppm. Somewhat surprisingly, then, the

La increase from 100 to 125 ppm had nothing to do with La addition in this hypothetical example. Conversely, if the rock gained mass, the concentration of La would be decreased. The key point is that the concentrations of immobile elements can change during metasomatism. For cases where the REE are immobile, REE patterns can be shifted up (rock mass loss) or down (rock mass gain) (e.g., Masters and Ague, 2005; Wagner et al. 2010; Fig. 2).

The complicating factor here is *closure*: the concentrations of all the constituents in the composition have to add up to 100 wt. % (within analytical error). Thus, due to the 100 % normalization constraint, changes in one oxide or element will impact one or more of the others (e.g., Chayes, 1949; 1971). Therefore, compositions are inherently multivariate, and statistical analysis of compositional data commonly benefits from multivariate statistical techniques (e.g., Aitchison, 1986; Woronow and Love, 1990; Ague and van Haren, 1996; Ague, 2011). The core of this multivariate approach is to use ratios of concentrations, not their absolute values. Because ratio statistics tend not to be Gaussian and for other technical reasons, it is better to work with the logarithms of ratios rather than the ratios themselves, but this is easily done. Note that expressing compositions in moles does not alleviate the closure problem, as the underlying closure correlations remain.

Relative and absolute chemical changes

Chemical changes can be determined in a relative or absolute sense. Assessing relative changes only requires consideration of elemental ratios, whereas some type of reference frame is required to assess absolute changes (see below).

Consider the increase in La/Lu along a metapelite layer approaching a fluid conduit in Figure 3a. There is no ambiguity regarding the precursor rock, so the change in ratio means

unequivocally that metasomatic changes have occurred. The percent change in ratio can be quantified, as can the statistical significance of differences in ratios between groups of samples (e.g., Woronow and Love, 1990).

The effects of metasomatism are undeniable in Figure 3a, but there are multiple (five) interpretations for what actually happened. (1) La was added and Lu was lost. (2) La was added and Lu remained constant. (3) La and Lu were both added, but La was added to a greater extent. (4) La and Lu were both lost, but Lu was lost to a greater extent. (5) La was constant and Lu was lost. For this example, the mass transfer followed (2), resulting in a nearly order-of-magnitude increase in Lu/La. Figure 3b depicts a decrease in Eu/Sm toward a fluid conduit in a metarbonate rock. Here, both Eu and Sm were gained, but Sm was gained to a greater extent.

For many purposes, the change in ratio is all that is needed to test a particular geologic hypothesis. On the other hand, to differentiate between the five possibilities for ratio change, some type of reference frame is needed to enable quantification of mass changes for each element individually. Three reference frames are available: (1) zero or known rock mass change; (2) zero or known rock volume change (e.g. Chowdhury et al. 2013; Centrella et al. 2016); and (3) zero mass change for an "immobile" element or elements.

The geochemical reference frame of option (3) is the most general and permits evaluation of rock mass, volume, and individual element changes. There have been many discussions of how best to select the geochemical reference frame to which the reader is referred (e.g., Grant, 1986; Brimhall et al. 1988; Ague, 1994a; 2003; Baumgartner and Olsen, 1995; Ague and van Haren, 1996; Penniston-Dorland and Ferry, 2008). Typical elements considered in this regard are the high-field strength elements (HFSE); Zr has received perhaps the most attention. Some commonly-employed elements, like Al and Ti, have limited mobility in some geologic settings,

but can be quite mobile in others. Using the REE as a reference frame without careful evaluation could be highly problematic as they can undergo significant transport despite being HFSE (see below). Moreover, in extreme environments, including some ultrahigh-pressure (UHP) rocks and zones of extensive partial melting, all or nearly all elements can be mobilized, thus limiting the utility of the geochemical reference frame approach. In what follows, the reference frame used in the original studies (option 1, 2, or 3) is also used herein unless otherwise noted. Statistical treatment of data follows Ague (2011).

Care must be taken when reading the classic paper by Grant (1986) which describes the "isocon" method for quantifying metasomatic changes. The method as employed in, e.g., Figure 2 of Grant (1986) is straightforward. However, it is also asserted that for immobile elements, the change in "geochemical concentration" is equal to zero (p. 1977). Such "geochemical concentrations" must not be confused with actual concentrations; as shown above, the concentrations of immobile elements ***must*** vary due to the closure constraint if there are overall rock mass changes. It follows that the concentrations of immobile elements will be unchanged only in situations where there has been no overall bulk rock mass change (e.g., 100 kg of starting rock is transformed into 100 kg of altered rock). However, this is not the general case in metasomatism.

A further important consideration is that physical mixing of rock types may produce a very different metasomatic signature than fluid infiltration. This can affect, for example, the metasomatic rinds on blocks within deforming subduction zone mélange (e.g., Bebout and Barton, 2002; Penniston-Dorland et al. 2014).

Finally, intrinsic variations in pre-alteration rock chemistry due to, for example, original sedimentary heterogeneities or igneous fractionation, may be large enough to obscure or mask the geochemical evidence for metasomatism (e.g., Penniston-Dorland and Ferry, 2008).

REE Behavior During Fluid-Rock Interaction

Rock types and patterns of REE mobility

The data set focuses on representative examples for which quantitative mass balance analysis is viable. These have direct relationships between precursors and their altered equivalents together with well-defined reference frames, as well as compositional data for a reasonably wide range of major, minor, and trace elements. Given these constraints, metasomatic studies that lack REE analyses, or that have REE and trace element analyses but lack major elements are, with two exceptions, not included in the data set. New studies are being published on a regular basis; unfortunately, some are too recent to be incorporated herein but it would be very instructive to include them in future updates to the data set.

To help facilitate discussion, rock types are subdivided somewhat arbitrarily into six broad categories. (1) Regional metamorphism including mostly Barrovian metamorphism of pelitic rocks but also mafic lithologies. (2) Regional metamorphism of carbonate rocks. (3) Subduction zone metamorphism including pelitic and mafic precursor rock types. (4) Subduction zone metamorphism of carbonate rocks. (5) Greenschist facies shear zones cutting granitic rocks, Mont Blanc Massif. (6) The final category comprises examples that do not fit neatly into the other categories: dynamothermal aureole (shear zone), magmatic/pegmatite fluid infiltration, and charnockite formation. The mass changes for many elements including the REE and other HFSE can be significant in this category, thus pushing the limits of mass balance-type analysis. The

charnockite example is from the classic locality at Kabbaldurga, southern India (Stähle et al. 1987), but is not intended to represent all forms of charnockite-related mass transfer. Rather, it is included as an illustration of strong HREE metasomatism (see below).

Patterns of REE mobility have also been subdivided, as follows. (A) Limited or no REE mobility. (B) Light REE mobility. (C) Heavy REE mobility. (D) Overall loss of REE. (E) Europium "anomalies". The quotation marks are employed to distinguish between the Eu mass changes due to fluid-rock interaction studied herein and other processes for which the term *Eu anomaly* is typically used such as igneous fractional crystallization. (F) Local redistribution of REE. Some overlap between categories is unavoidable as samples may be characterized by multiple patterns of metasomatism.

The element with the maximum mass change is referred to as REE_{Max} (values are given in Table 1). The most common REE_{Max} elements are La, Yb-Lu, and Eu; they are associated primarily with LREE, HREE, and Eu "anomaly" mass transfer, respectively, and account for about half of the total. For the remainder, all REE except Nd and Er are found as REE_{Max}. These relationships should not be taken as representative of all natural systems, as the data set is not a statistical sampling of every form of REE mass transfer.

Graphical representation of chemical changes

Two types of plots are used extensively in this paper. The first type is percentage mass change diagrams for REE and other selected elements (Figs. 4, 6, 8, 10, 12, 14). Some data sets have small numbers of samples that may not fully represent the chemical variability of precursors or their altered equivalents, thus limiting the amount of statistical analysis that can be done. In some cases, only one precursor and one altered analysis are available. When they can be

calculated, ±2σ standard errors on average mass change values are shown. It is very important to point out that these are not chondrite-normalized plots, but rather depictions of elemental percentage mass change (mass gains are positive, losses negative). The second type of plot was developed herein and is referred to as a "bar code" diagram. These display percentage mass changes using a color-coding scheme (Figs. 5, 7, 9, 11, 13). Given the statistical limitations noted above, the mass changes are grouped into broad ranges that attempt to capture the general patterns of metasomatism while avoiding unwarranted detail that could lead to overinterpretation.

Immobile or limited mobility of REE

While the data set is not a statistically-comprehensive survey of all types of REE mobility, more examples (about 1/3) fall into this group than any other and include all the rock type categories noted above except category (6) (Figs. 4, 5). Thorium mobility is very rare in this group, as it is in most others. On the other hand, there are several examples of significant U metasomatism in subduction (LM7–LM9) and shear zone settings (LM13). Two examples underwent large P mass changes (LM2, LM11), but most did not. However, although mean P mass changes may be indistinguishable from zero statistically, 2σ uncertainties can be large which suggests local scale redistribution of P even though it was not lost or gained overall. Yttrium was mostly immobile in these examples, although several display small gains or losses. Importantly, a wide array of other major and trace elements were mobile, illustrating that significant rock chemical alteration is possible without strongly affecting the REE (Fig. 5). The patterns of element mobility vary considerably, but most samples lost considerable LILE.

Mobility of the LREE

Most examples gained LREE, but losses are also observed (Figs. 6, 7). For samples that gained LREE, enrichments can be extreme and in some cases exceed +1000 %. Where data are available, these LREE gains are commonly associated with phosphates, particularly monazite and/or apatite; allanite can be another important LREE host in this group (Pan and Fleet, 1996). Gains of P, Y, or both are consistent with LREE concentration in phosphate phases. Most of these rocks lack garnet or other phases that would concentrate the HREE. For example, LREE2 has only 1-2 volume % garnet. Loss of HREE and Y due to hornblende breakdown to biotite in the dynamothermal ophiolite aureole example (LREE6) is inferred to have been offset by HREE gains due to garnet growth (Dostal et al. 1980). In addition, the rock gained substantial Zr, Th, and U, so growth of metasomatic zircon may also have helped offset HREE losses. Although not specified in the original paper, the large gains in P strongly suggest that LREE gains were associated with a phosphate phase or phases. The LREE loss examples are also associated with phosphates. For example, LREE5 lost P and contains irregular monazite grains interpreted to be corroded relics. In addition, this example preserves remnants of allanite in kyanite; this could also have contributed to LREE loss.

All examples underwent various forms of major and minor element metasomatism; clearly, REE transport did not occur without the mobilization of other elements as well (Fig. 7).

Calculated mass additions for LREE2 increase smoothly with decreasing atomic number implying systematic open system behavior. However, it should be noted that due to uncertainties in the LREE2 geochemical reference frame and intrinsic sample heterogeneity, it is debatable if the LREE mass additions calculated herein for this example are in fact significant (Penniston-Dorland and Ferry, 2008). Nonetheless, reference frames using Al, Ti, and two Zr measurements

(XRF or ICP-MS) yield a mean mass change for La of 52.4% ± 6.4% (2σ standard error), an uncertainty roughly the size of the data symbols in Figure 7.

Mobility of the HREE

Gain of HREE is the most commonly observed pattern in this group (Figs. 8, 9). Where data are available, this was due mainly to the growth of garnet or xenotime; hornblende and sphene may also have been important in some instances (Fig. 8). Gain of HREE is commonly coupled to gain of Y, which is unsurprising given the importance of phases like garnet or xenotime in the chemical alteration. Phosphorous behavior is more variable. Example HREE9 that interacted with pegmatite fluids gained Th. Metasomatic apatite in this sample contains Th (Carson and Ague, 2008), and it was also likely hosted by allanite (e.g., Hermann, 2002). Otherwise there was little Th mobility in this group. HREE9 also gained U, but the mineral host is uncertain. The example of incipient charnockite formation (HREE10) has the most striking REE losses, attributed to zircon, apatite, and monazite destruction by Stähle et al. (1987).

Many other major and trace elements were mobile but they do not vary systematically with HREE mass changes (Fig. 9).

Overall loss of REE

Examples which lost all REE are less common than others in the data set (Figs. 10, 11). They span a diverse range of settings: subduction complex, magmatic-hydrothermal fluid alteration, charnockite, and Barrovian metapelite. The subduction examples involve high fluid fluxes and infiltration of fluids with low solute loads capable of dissolving REE and destroying REE carriers including epidote, titanite, garnet, and/or phosphates (John et al. 2008; van der Straaten et al. 2008). The magmatic-hydrothermal fluid example is highly altered metapelite consisting mostly of sillimanite, muscovite, and graphite at the contact with pegmatite and

associated quartz veins. REE loss is inferred to be the result of apatite, monazite, and garnet destruction during alteration. The Barrovian example is a plagioclase-rich alteration selvage adjacent to a quartz vein. Garnet breakdown led to HREE and Y loss, and there is considerable evidence for overgrowths on, and dissolution-reprecipitation of, apatite which likely affected the LREE and mid REE (MREE) (Masters and Ague, 2005; Ague and Baxter, 2007). As noted above, loss of REE during incipient charnockite formation was attributed to zircon, apatite, and monazite destruction by Stähle et al. (1987). All examples lost P, Y, and U; extreme fluid-rock interaction even caused Th loss in two cases. No discernible correlations of REE behavior with that of other elements are evident (Fig. 11).

Fluid-rock interaction and europium "anomalies"

The precipitation or breakdown of plagioclase or lawsonite largely control gains or losses of Eu with respect to other REE. These Eu mass change "anomalies" are here subdivided into four categories (Figs. 12, 13). (1) Fluid-rock interactions that destroy plagioclase can deplete Eu, whereas those that produce plagioclase can enrich it. For example, in Eu1, plagioclase and garnet grew in response to fluid infiltration. The growth of garnet is inferred to have produced the Y enrichment. Minor to moderate losses of some REE in this example may have resulted from phosphate mineral destabilization. In Eu2, plagioclase was destroyed, leading to a negative "anomaly". (2) The precipitation of plagioclase from vein-forming metamorphic or pegmatitic fluids progressively depletes the fluids in Eu relative to neighboring REE. Consequently, these Eu-depleted fluids can produce metasomatic REE patterns characterized by negative Eu "anomalies" in the rocks they infiltrate (Eu3, Eu5, Eu6), even if the infiltrated rocks lack plagioclase (e.g., Eu3; Ague, 2003; Carson and Ague, 2008). Profiles across zones of altered rock adjacent to conduits for such fluids commonly show progressively deepening Eu

395 "anomalies" as the conduits are approached (Eu3). (3) Redistribution of Eu among feldspars
396 resulting in little or no overall Eu mass change. For the charnockite example (Eu7), the positive
397 Eu "anomaly" is very distinct relative to the other REE, most of which were lost due to
398 destruction of apatite, monazite, and zircon (Stähle et al. 1987). (4) Preferential enrichment of Eu
399 is also observed in metasomatic lawsonite (Eu6; Vitale Brovarone et al. 2014). Oxygen fugacity
400 is not quantified for all the examples so its role remains to be established.

401 Most of the examples gained Y, whereas P behavior was more variable. U was either
402 immobile or was gained; both Th and U were added to two examples at pegmatite contacts (Eu5,
403 Eu6).

404 **Local redistribution of REE**

405 Local-scale transport of REE can also occur within a rock mass; two examples are shown
406 in Figure 14. Average mass changes converge to around zero with a large standard deviation
407 indicative of local redistribution. Fluid flow was highly channelized in both the subduction
408 example (R1,2) and the granitic shear zone example (R3,4). For the subduction case, HREE loss
409 due to reaction of pre-existing rutile and sphene was followed by HREE reincorporation into
410 newly-grown garnet (Beinlich et al. 2010). For the shear zone, LREE losses were associated with
411 alteration of protolith magmatic minerals whereas gains resulted from precipitation of new
412 LREE-bearing phases (e.g., monazite, bastnäsite, aeschynite and tombarthite; Rolland et al.
413 2003).

414

415 **Geochemical Relationships Among Elements**

416 **Neighboring REE**

Neighboring REE, such as La-Ce, Sm-Nd, and Yb-Lu, are strongly positively correlated along 1:1 percentage mass change lines (Fig. 15). The LREE have the largest range of mass changes (Fig. 15a). The HREE have a notably smaller range but nonetheless can undergo considerable mobility (Fig. 15d). Europium mass change "anomalies" are clearly discernible when plotted with respect to neighboring Sm (Fig. 15c). Aside from this Eu behavior, a key point to emphasize is that adjacent REE are in most cases mobilized together. It follows that constancy of neighboring REE ratios does not mean that the elements were immobile.

Phosphorous and Yttrium

Mass changes for La (a representative LREE) correlate positively with those for P (Fig. 16a). Similar relations hold for REE_{Max}-P, although there is somewhat more scatter (Fig. 16b). On the other hand, there is considerable scatter in HREE (Lu)-P mass changes, and the positive correlation between them is very weak at best (Fig. 16c). Mass change relations for P-Y are quite scattered as well, although there is a dispersed positive correlation (Fig. 16d). Positive correlations between Lu-Y and REE_{Max}-Y, however, are much stronger, remarkably so for REE_{Max}-Y (Figs. 16e, f).

Five samples fall off the REE_{Max}-Y 1:1 correlation line (Fig. 16f). The REE_{Max} elements for the four non-metacarbonate examples are in the LREE (e.g., La); they underwent large P gains as well. The LREE mass changes are less strongly linked to Y changes than the MREE or HREE. Two of these five nonetheless also gained significant Y. The metacarbonate sample (HREE3) has strong gains of HREE, Y, and P.

Thorium, Uranium, and Niobium

Thorium is largely immobile or nearly so for most rocks (Figs. 17a, b). Only five examples display clear Th mass transfer. (1) A mylonite shear zone in a dynamothermal aureole

below an ophiolite remnant that channeled high-*T* fluids (LREE6; Figs. 6, 7). (2, 3) Two examples of orthogneiss infiltrated by magmatic-hydrothermal fluids exsolved from pegmatite dikes (Eu6/HREE9 and Eu7; Figs. 12, 13). (4) Graphitic sillimanite-muscovite rock derived from metapelite adjacent to or incorporated into a pegmatite-quartz vein complex (LOSS2; Figs. 10, 11). (5) High-*P* (HP) or possibly ultrahigh-*P* (UHP) eclogite facies veins derived from blueschist by prograde devolatilization (LOSS3; Figs. 10, 11). Glaucophane, dolomite, and sphene were replaced by omphacite, garnet, and rutile; ~75% of the rock's total carbon was released as CO_2 to infiltrating fluids (John et al. 2008). In summary, four of the five examples involve aureoles and/or magmatic-hydrothermal fluids, and the fifth is from a HP (UHP?) setting in a subduction zone.

A plot of Th-U mass changes shows that U is more mobile than Th such that U mass transfer can occur without mobilization of Th (Fig. 17a). This is consistent with experimental evidence showing higher U solubilities relative to Th in aqueous fluids given sufficiently elevated oyygen fugacity and/or salinity (e.g., Bailey and Ragnarsdottir, 1994; Bali et al. 2011). In the five examples for which Th was mobile, however, a very clear positive correlation of U-Th mass changes exists (Fig. 17a). Furthermore, for these rocks, the positive correlation between Th and REE_{Max} mass changes is also strong (Fig. 17b). Thus, Th mobilization did not occur without U and REE mobilization in the studied samples.

Mass changes for U and REE_{Max} tend to be associated, although there is considerable scatter (Fig. 17c). U and Nb mass changes appear to be roughly correlated (Fig. 17d); in the subduction rocks, this may reflect some control of U-Nb geochemical systematics by rutile (e.g., Rudnick et al. 2000).

463 **Alkalis and Alkaline Earths**

464 Relationships among selected alkali and alkaline earth elements are shown in Figures 18–
465 20. Loss of K together with Na is common (Fig. 18a). Coupled Na gain and K loss, as well as K
466 gain and Na loss, are also observed. Remarkably, however, there are no examples of both
467 significant Na and K gain. Overall, there are many more examples of K loss than K gain in the
468 data set, although it is possible that this reflects some degree of sampling bias.

469 Geochemically, Ca commonly behaves similarly to Na giving rise to sodic-calcic
470 metasomatism in crustal settings (e.g., Battles and Barton, 1995; de Jong and Williams, 1995;
471 Ague, 1997). For non-subduction zone rocks, there is a general positive correlation between Na
472 and Ca mass changes, reflecting the important control of plagioclase as a host for these elements
473 (Fig. 18c). One low-grade metacarbonate example diverges strongly from the trend as it contains
474 albite-rich feldspar (HREE3). As expected on geochemical grounds, Ca and Sr mass changes are
475 positively correlated (Fig. 18e). Thus, although they differ in detail, Ca-K and Sr-Rb systematics
476 resemble those for Na-K, with few or no examples of coupled Ca-K gain or Sr-Rb gain (Figs.
477 18b, f).

478 Subduction zone rocks, on the other hand, display no Na-Ca correlations, although the
479 lack of examples of simultaneous Na-Ca gain is conspicuous (Fig. 18d). In subduction settings,
480 Na and Ca are not closely coupled in plagioclase, but instead are distributed across multiple
481 phases (e.g., lawsonite, glaucophane, omphacite, garnet, epidote) facilitating a range of behavior.
482 The subduction metacarbonate examples are distinct. Their strong Na-gains reflect growth of
483 sodic phases such as glaucophane, omphacite, and pectolite (LM11, LM12, HREE8). Calcium
484 loss in two of these examples resulted from stoichiometric carbonate mineral dissolution
485 occurring simultaneously with silicate precipitation (Ague and Nicolescu, 2014). The dissolved

carbonate species are transported away from the site of reaction and may precipitate elsewhere in the subduction zone (e.g., Piccoli et al. 2016; Scambelluri et al. 2016). The liberated Ca could also potentially drive calcic metasomatism and the growth of Ca-bearing silicates including lawsonite (e.g., Alberto Brovarone et al. 2014) or clinopyroxene (e.g., LM10, in which glaucophane broke down and Ca-bearing sodic clinopyroxene grew).

Excellent positive correlations exist between mass changes for K and those for the geochemically-similar trace elements such as Rb hosted largely by micas and/or K-feldspar (Fig. 19a). Correlations among K, Ba, and Cs are similar (not shown). Pb mass changes do not correlate well with these elements, but do show a positive relationship with Sr mass changes, indicating significant coupling of Sr-Pb behaviors (Fig. 19b). For non-subduction zone rocks, this is probably due to growth or breakdown of plagioclase. The large Pb gain recorded by LM8 that falls off the general trend is inferred to be related to Pb incorporation into abundant sulfide minerals (mostly pyrite and chalcopyrite). The three examples plotting well above the trend are characterized by extensive lawsonite (Eu4, Eu5) or epidote metasomatism (LM1). REE_{Max} mass changes (or those of individual REE) do not vary in any clear systematic way with Rb, Sr, K, Ba, Cs, Ca, or Na mass changes overall across the dataset (not shown).

Volatiles, REE, and Alkalis

REE_{Max} mass changes relative to those of the major volatiles are shown in Figure 20a. The bulk of the volatile data are actually X-ray fluorescence loss on ignition values, which serve as proxies mostly for H_2O and CO_2 contents (but also include organic matter oxidized during analysis and other complications). Data for actual H_2O and CO_2 contents, as well as other volatiles including F, S, and Cl, are available for some examples but are not treated separately as

509 they are not determined in most analyses. The REE_{Max}-volatile mass changes range widely and
510 all fields of the mass change diagram are occupied. The patterns for La, Sm, and Lu differ, as
511 expected given the differing mass changes for LREE, MREE, and HREE (Fig. 15), but
512 systematic trends with volatile mass changes are not obvious (not shown).

513 Alkali metal behaviors relative to rock volatile gain or loss are shown in Figure 20b. For
514 rocks that lost volatiles, only two main types of Na-K behavior are observed: 1) gain of Na and
515 loss of K or 2) loss of both Na and K. For rocks that gained volatiles, gain of K and loss of Na is
516 also possible, in addition to the two other types (Fig. 20b). As noted above, the lack of any
517 examples that gained both K and Na is striking. Ca-K and Sr-Rb systematics are similar to those
518 of Na-K (not shown). Figure 20b illustrates that K is generally lost when volatiles are lost (also
519 the case for Ba, Cs, and Rb). Potassium and related elements can also be lost if volatiles are
520 gained. Notably, however, volatile gains were required to add K to the rocks of the dataset,
521 coupled to Na loss (Fig. 20b).

522

523 **Discussion**

524 The mobilization of REE is always accompanied by the mobilization of an array of other
525 non-REE major and trace elements. On the other hand, numerous examples exist of extensive
526 mobilization of non-REE without significant open-system transport of the REE. The patterns of
527 REE transport show no clear correlations with the general form of major element metasomatism,
528 such as Si-Al, Mg-Fe, or alkali-alkaline earth metasomatism (Figs. 5, 7, 9, 11, 13). Of course, for
529 individual examples, there is coupled mass transfer among elements, but with the exception of P
530 and Y (see below) the overall lack of systematic relationships across the entire data set is
531 striking.

532 The mobilization of REE is, however, a strong function of the growth or breakdown of
533 REE-bearing phases. Given the wide range of rock types investigated, the number of key phases
534 is notably small. Mass transfer involving LREE and MREE in the data set was dominated by
535 reactions involving apatite, monazite, and allanite/epidote-group minerals; rarer phases including
536 Ca-LREE-fluorocarbonates can also be important. Metasomatism involving plagioclase or
537 lawsonite determines Eu mass change "anomalies" relative to neighboring REE. Metamorphic
538 HREE systematics are controlled largely by garnet and xenotime. Contributions from
539 hornblende, rutile, sphene, extremely REE-rich phases like tombarthite, and in rare cases even
540 zircon are documented as well.
541 The REE are locally redistributed among phases, in closed or open systems, and can be
542 added or lost from rocks during fluid-rock interaction. REE-bearing phases that precipitate take
543 REE out of fluids, whereas those that breakdown release REE. One possibility is that the host
544 phase is already present in the rock. For example, garnet that grows during infiltration could pick
545 up HREE and Y and thus add them to the bulk rock (e.g., HREE1). Garnet breakdown would do
546 the opposite (e.g., LREE6). Another possibility is that fluid-dominated metasomatism is so
547 extensive that new REE-bearing phases are produced. Examples include the growth of xenotime
548 associated with P and Y metasomatism and the consequent enrichment of HREE (HREE3), and
549 the growth of monazite, bastnäsite, aeschynite and/or tombarthite in example LREE8.
550 REE and P mass changes are broadly correlated (Figs. 16a, b). This reflects the
551 importance of phosphate minerals—mainly apatite, monazite, and xenotime—to REE
552 metasomatism in many examples. Furthermore, REE_{Max} mass changes for most rocks have an
553 extremely strong positive correlation with Y mass changes (Fig. 16f). The excellent 1:1
554 correlation reflects coupling of HREE or MREE mass changes to Y mass changes. Yttrium and

555 the HREE are hosted largely by the same phases (garnet, xenotime), leading to strong Y-HREE
556 covariance. In addition, the ionic radius of Y^{3+} is very similar to the MREE (e.g., Gd^{3+}), yielding
557 Y-MREE correlations. Five samples whose maximum REE gains are in the LREE fall off the 1:1
558 REE_{Max}-Y correlation line (Fig. 16f). This reflects the strong controls exerted by phases such as
559 apatite and monazite on LREE budgets. Apatite and monazite can contain considerable Y, so Y
560 metasomatism can take place concurrently; indeed, three of these five examples gained Y in
561 addition to LREE.

562 Notably, the uncertainties on mean P mass changes are commonly larger than those for
563 other elements (Fig. 16). Phosphorous mass changes that are statistically indistinguishable from
564 zero but with very large error bars are consistent with significant local redistribution that did not
565 necessarily transport P into or out of the rock. Interface coupled dissolution-reprecipitation (e.g.,
566 Putnis and Austrheim, 2010; Putnis and John, 2010) is one process by which this could happen
567 that has implications for the REE systematics of phosphates (e.g., Harlov et al. 2011). For
568 example, dissolution of original grains would release phosphate-hosted REE to infiltrating fluids
569 whereas reprecipitation could incorporate a new suite of REE depending on fluid chemistry.

570 The REE are typically fractionated by metasomatism. More or less equal amounts of REE
571 mass transfer are evident for some REE loss examples, but are otherwise rare. Mobility of just
572 one or several REE is also uncommon; it is only observed herein for an example of Eu
573 sequestration in plagioclase (Eu1). The fractionations reflect the preferences that the dominant
574 REE-host minerals have for particular REE or suites of REE, such as garnet for HREE,
575 plagioclase for Eu^{2+}, and so on.

576 REE metasomatism shows no simple correlations with major volatile (H_2O, CO_2) loss or
577 gain, but rather a range of behaviors (Fig. 20a). Coupled volatile addition and REE loss suggests

leaching by infiltrating fluids. Loss of fluids carrying REE during prograde devolatilization may have resulted in combined REE and volatile loss. In addition, prograde volatile loss can be driven by infiltration; this could have either removed REE, or added them depending on fluid composition and mineralogy. A number of rocks also underwent REE mass transfer with relatively little overall volatile mass change (Fig. 20a), so in some cases fluids move in and out of rocks transporting REE without dramatically altering rock volatile contents.

The lack of clear correlations between REE mass changes and mass transfer of major volatiles (H_2O, CO_2) or most non-REE elements (except P) suggests that mechanisms of REE transport differ to some degree from those controlling other mobile constituents. Many REE carriers have been shown or postulated to be in fluids, including F, Cl, carbonate, hydroxide, and sulfate species; other variables including oxygen fugacity (for Eu) and pH can also play important roles (e.g., Michard and Albarède, 1986; Gieré, 1990; Bau, 1991; Gruau et al. 1992; Gammons et al. 1996; Pan and Fleet, 1996; Bao et al. 2008; Harlov, 2012; Manning and Aranovich, 2014). For example, LREE gain in example LREE1 was the result of Ca-REE-fluorocarbonate precipitation, indicating a likely role for F and carbonate anions in REE transport. Halogen carriers are commonly inferred, but given that Cl complexes can transport major elements including alkalis and alkaline earths, it is somewhat puzzling that clear, systematic relationships among these elements and the REE are not evident in the data set. In addition to the above possibilities, observed correlations between REE and P and/or Y mass changes could be due to REE transport by P and/or Y complexes, or transport of these elements together by some other complexing agent (e.g., Gieré, 1990; Lee and Byrne, 1992; Ague, 2003; Carson and Ague, 2008).

600 It is interesting to note that the strong HREE loss for the charnockite example (HREE10)
601 differs from the bulk of the data set (Fig. 8). This may reflect fluids with reduced water activity
602 due to the role of CO_2, brines, and/or melt in charnockite and granulite genesis (e.g., Newton et
603 al. 1980; Valley et al. 1990; Harlov, 2012; Rajesh and Santosh, 2012; Manning and Aranovich,
604 2014), as distinct from predominantly aqueous metasomatic fluids for the other rocks.
605 Major gaps in knowledge remain regarding how dissolved REE are transported in fluids
606 that need to be addressed by new field, fluid inclusion, experimental, and theoretical studies.
607

608 ## Implications

609 ### Implications for High Field Strength Elements

610 The data set has clear implications for the mobility of REE and high field strength
611 elements (HFSE). The conventional wisdom is that the REE are relatively immobile in
612 metamorphic fluids. This is indeed the case for roughly 1/3 of the data set. As these examples are
613 all from high-flux environments which mobilized other elements, one would expect little REE
614 mobility in lower flux, less channelized environments as well. Some high flux environments,
615 however, are conducive to REE transport, and examples are shown for all settings considered
616 including Barrovian and subduction zone metamorphism. Moreover, under such circumstances,
617 the REE are typically the most mobile of the elements traditionally considered to be refractory
618 including the HFSE (Fig. 21).
619 On a percentage mass change basis, these elements listed in order of decreasing mobility
620 are: REE>U>Nb>Ti>Th~Zr (Fig. 21). This mobility of REE is broadly consistent with recent
621 experimental results relevant for subduction (Tsay et al. 2014), but more work is clearly needed
622 across a range of settings. Uranium mobility is no doubt influenced by redox state, with higher

623 solubilities expected for more oxidizing conditions (e.g., Bailey and Ragnarsdottir, 1994; Bali et
624 al. 2011). Nb displays less, but still considerable mobile behavior, in accord with experimental
625 evidence (particularly in halogen-rich fluids; e.g., Tanis et al., 2015). Rutile, a major host for Nb,
626 has been observed in veins and other metasomatic structures (e.g., Ague, 2003; Gao et al. 2007 ;
627 Spandler et al. 2011). Care must be exercised, however, to determine if the Ti and Nb were
628 transported over great distances, or locally from wallrock to vein (e.g., Ague, 2014).
629 At the lowest mobility end of the spectrum, Th and Zr are largely immobile, at least in
630 the water-dominated fluids studied herein. The lower degrees of mobility of Zr or Th relative to,
631 e.g., Ti, is well established by experiment (e.g., Hermann and Spandler, 2008; Tsay et al. 2016).
632 It is true that Zr and/or Th are used as reference frame elements in quite a few of the studies, but
633 they are not used in all of them and, furthermore, Zr-Th behavior is in most cases strongly
634 coupled which would not be expected if one or both were mobile. The much larger degree of U
635 mobility relative to Th can account for at least some of the isotope disequilibrium commonly
636 observed in arcs, including Tonga-Kermadec, Mariana, and Sunda (e.g., Turner et al. 2001). The
637 largest degrees of element mobility recognized herein for Th and Zr, as well as other HFSE, are
638 found in magmatic/magmatic hydrothermal settings as well as the dynamothermal shear zone
639 aureole, charnockite, and HP (UHP?) rocks (Fig. 17a). The well-known mobility of, for example,
640 Th and U from charnockite and other granulite facies terranes is consistent with this pattern (e.g.,
641 Rollinson and Windley, 1980; Hansen and Harlov, 2007; Raith et al. 2016).
642 Notably, one example of HP (UHP?) rock shows considerable HFSE depletion (LOSS3,
643 Table 1; John et al. 2008). It is tempting to hypothesize that this mobility could have been aided
644 by solution of refractory phases into supercritical fluids intermediate between aqueous fluids and

hydrous melts at extreme pressures (e.g., Manning 2004; Ferrando et al. 2005; Hermann et al. 2013).

Implications for Garnet and the HREE

Garnet has considerable potential to sequester HREE and Y, incorporating these elements from fluids during growth. Garnet is also nearly ubiquitous in medium and high grade regional metamorphic settings. These relationships imply that fluids exiting such settings ascending into shallower parts of the lithosphere will carry with them a geochemical fingerprint depleted in the HREE and Y. Although speculative, perhaps this helps explain why many REE ores are noticeably depleted in the HREE (e.g., Long et al. 2010).

Implications for LILE and Alkali Systematics

Coupled gain of K and loss of Na is observed mainly for rocks that gained volatiles, consistent with retrograde down-temperature (down-*T*) flow which tends to add K and remove Na (e.g., Brimhall, 1977; Dipple and Ferry, 1992), or infiltration of fluids from K-rich sources (e.g., pegmatites, micaceous metasediments) (Fig. 20b). Coupled K gains and Na losses are observed for down-*T* flow in the dynamothermal aureole shear zone (LREE6), flow of magmatic-hydrothermal fluid from K-rich pegmatite into feldspathic orthogneiss (Eu7), retrogression of eclogite to blueschist (LOSS4), and replacement of plagioclase by K-feldspar in charnockite (Eu8/LOSS5/HREE10).

Leaching of both K and Na are possible during fluid-rock interaction associated with either prograde devolatilization, or volatile gains. In either case, large fluid fluxes are likely required to drive the alkali metasomatism (e.g., Yardley, 1986; Bucholz and Ague, 2010; Ague, 2011).

667 Importantly, if K and related elements are mobilized during prograde devolatilization,
668 then they are lost, reflecting transport of these elements out of rocks by escaping fluids (Fig. 20b)
669 (e.g., Melzer and Wunder, 2000), up-*T* fluid flow that also produces Na ± Ca gains (e.g., Dipple
670 and Ferry, 1992; Ague, 1997), strong alkali leaching (e.g., Yardley, 1986), and/or flow across
671 lithologic contacts (e.g., Ague, 2003; Breeding et al. 2004; Ague and Nicolescu, 2014; Galvez et
672 al. 2013) (Fig. 20b). Examples include the destruction of micas and growth of plagioclase (e.g.,
673 Eu1, HREE3) or, in subduction zones, the destruction of phengite and the growth of glaucophane
674 and/or omphacite (e.g., LM11, LM12, HREE8).

675 **Comments on LILE and HFSE in Arcs**

676 An important general feature of arc magmas are the elevated concentrations of LILE
677 relative to HFSE. In particular, the relative "depletion" of Nb relative to K and related LILE has
678 been extensively studied (e.g., Kelemen et al., 1993). Fluids tend to remove K, Rb, Ba, and Cs
679 during prograde devolatilization in high flux zones, and thus have the potential to deposit these
680 elements elsewhere as they migrate along flow paths. As a consequence, fluids ascending from
681 subducted crust (mafic or metasedimentary) are likely an important source of LILE enrichment
682 in arcs (e.g., Stolper and Newman, 1994; Noll et al. 1996; Schmidt, 1996; Johnson and Plank,
683 1999; Becker et al. 2000). Furthermore, these fluids would in general lack HFSE including Nb,
684 Ti, Th, and Zr, consistent with the observed relative depletions in these elements.

685 At higher temperatures involving partial melting, HFSE including Th are mobilized (e.g.,
686 Johnson and Plank, 1999). Zircon solubility in silicate melts is considerable, leading to increased
687 zircon destabilization as temperature increases (e.g., Boehnke et al. 2013). Moreover, Zr
688 partitions into coexisting rutile with increasing temperature (e.g., Zack et al. 2004; Watson et al.
689 2006; Tomkins et al. 2007), further destabilizing zircon. Indeed, at ultrahigh-temperature (UHT)

conditions in metasedimentary systems, zircon can be completed destroyed (e.g., Kelsey and Powell, 2011). This is likely the case in more mafic bulk compositions as well, but more work remains to verify this. Because rutile, a major Nb host, can remain stable during partial melting, the Nb and Ti anomalies relative to LILE in arcs could be preserved, even though HFSE associated with zircon (e.g., Zr, Th, Hf) could be strongly mobilized.

Implications for Geochronology

The mobility of Nd, Sm, and Lu has implications for geochronology (Hf data are missing for many examples and are not considered further). Significant mass changes for Sm and/or Nd are present in about 50% of the data set examples; there are fewer examples of Lu changes but mobilization is clearly possible (Figs. 15b, d). Garnet-whole rock Sm/Nd or Lu/Hf geochronology could be affected if, for example, matrix REE values were modified after garnet growth. Whole-rock isochrons (e.g., O'Neil et al. 2012) could be disrupted by scatter or other irregularities if some rocks underwent open-system REE transport and others did not. Pervasive REE metasomatism can take place in large scale, shallow hydrothermal systems (e.g., Hellman et al. 1979; Windrim et al. 1984; Bartley, 1986; Gruau et al. 1992; Marsh et al. 2012). But at higher grades of metamorphism at greater depths, mobility appears to be more localized around, for example, high fluid flux conduits, as discussed herein. Nonetheless, diffusional exchange of Nd and other REE can take place across lithologic contacts, even in environments that did not undergo large fluxes (e.g., Watson and Baxter, 2007). Regardless of mechanism, in most cases Sm and Nd will not be differentially mobilized, such that bulk Sm/Nd ratios remain relatively constant even though considerable mass transfer of both elements may have occurred (Fig. 15b).

Implications for Petrotectonic Geochemical Discrimination Diagrams

712 Geochemical discrimination diagrams have proven to be invaluable for deducing tectonic
713 settings of magmatism (e.g., Pearce and Cann, 1973; Pearce et al. 1984). Many of these diagrams
714 focus on HFSE, due to their general resistance to alteration. As HFSE can be mobile, however, it
715 is illustrative to see what impact this would have on interpretations of tectonic settings. Consider
716 two examples: the Nb-Zr-Y diagram for mafic rocks (Meschede, 1986), and the Nb-Y diagram
717 for granitic rocks (Pearce et al. 1984). The concentrations of Nb and Y were varied within mass
718 change ranges compatible with Figure 21; Zr was taken to be immobile. Figure 22 shows that
719 this level of variation can skew considerably the field a given rock will plot in. Plotting positions
720 can shift over two, three, or more fields. These results illustrate that immobility of HFSE cannot
721 be taken for granted in petrotectonic studies; this fact becomes increasingly evident as the body
722 of quantitative mass balance studies grows. Appropriate criteria for selecting the least altered
723 rocks are essential to implement, as emphasized by, for example, Pearce (1996).

724 **Implications for Major Element Metasomatism During Regional Metamorphism of Pelites**

725 Given the remarkable utility of metapelitic mineral assemblages to elucidate
726 metamorphic grade (Barrow, 1893; 1912; Thompson, 1957), the chemical evolution of
727 metapelites during progressive Buchan or Barrovian metamorphism has long been a topic of
728 interest (e.g., Shaw, 1956). It remains relevant today, as pseudosections are typically constructed
729 for systems closed to non-volatile major element mass transfer. Nonetheless, focused flow in and
730 around veins may result in alkali and alkaline earth mass transfer that can stabilize index
731 minerals such as garnet (Ague, 1997) or staurolite and kyanite (Ague, 1994b, 2011; Bucholz and
732 Ague, 2010). Based on a statistical examination of over 350 rock chemical analyses from the
733 literature, Ague (1991) concluded that during progressive metamorphism: (1) in addition to
734 volatiles, significant silica may also be lost; (2) K is commonly lost; and (3) Na and Ca can be

735 mobile and be either gained or lost. The data set of the current study is useful to test these
736 findings as it is completely independent of the 1991 data set noted above.

737 Figure 23a confirms the silica loss, and also shows that increasing silica loss is correlated
738 with increasing volatile loss. Even if REE were immobile, they can still undergo considerable
739 concentration increases due to silica loss (Fig. 2). Previous studies have demonstrated that much
740 or all of this silica loss is local, being the result of mass transfer down chemical potential
741 gradients from altered wallrock selvages to adjacent veins. Vein mass balance, however, clearly
742 indicates that more silica is in the veins than can be accounted for by local loss, demonstrating a
743 role for fluid flow in precipitating exogenous silica. Such silica precipitation will in general
744 result from down-temperature flow (Ferry and Dipple, 1991). The fraction of external silica has
745 been found to be in the range of ~30 to >90% (Ague, 1994, 2011; Penniston-Dorland and Ferry,
746 2008; Bucholz and Ague, 2010). Silica can thus be added overall at the outcrop or larger scales
747 (e.g., Ferry, 1992; Breeding and Ague, 2002). If, however, the amount of veining is small, it
748 follows that overall silica additions are modest (e.g. Dasgupta et al. 2009). In addition, one
749 example in the data set gained considerable silica and volatiles (LREE1). It is a heavily altered
750 and silicified wallrock inclusion directly within a vein; it records large fluxes of fluid capable of
751 precipitating exogenous silica.

752 The loss of K and the variable loss or gain of Na and Ca are evident in Figures 23b and
753 23c. To first order, these systematics reflect destruction of micas (Fig. 23b) and Na-Ca mass
754 transfer largely controlled by plagioclase (Fig. 23c). The example of Ca gain and Na loss
755 (HREE1) which plots off the general trend in Figure 23c reflects destruction of feldspar together
756 with uptake of Ca by garnet. The mobility of these elements can, if large enough, help to
757 determine the stability of aluminous phases including chloritoid, garnet, staurolite, and kyanite

relative to micas and feldspars. Behavior can vary widely; in the low-pressure region of the Barrovian zones, Na-Ca metasomatism, K loss, mica destruction, and feldspar growth was widespread (e.g., LM1–LM3; LREE1). On the other hand, in some other Barrovian settings (e.g., Unst, Shetland Islands, Scotland; Wepawaug Schist, Connecticut) alkali loss and variable Ca behavior are typically observed (e.g., LREE3, LREE4; HREE1). The reasons for these differences remain as important research questions; it is interesting to note in this context that the two latter examples are higher-pressure (~0.8-1.0 GPa) than the first (~0.4-0.5 GPa).

The above are broad patterns, but other behavior is of course possible, such as K gain due to large down-temperature fluid fluxes (e.g., van Haren et al. 1996). Moreover, a wide array of other elements can be mobilized, including Al, which can be added to vein-selvage systems (e.g., Figs 7, 9). Regardless of the elements mobilized, the most pronounced effects are found adjacent to conduits such as veins. In regions impoverished in fluid flow due to channelization, or in settings very distal to conduits, much less transfer would be expected. Interestingly, regions of low fluid flux resulting from channelization will tend to border conduits, leading to the non-intuitive conclusion that regions of highest and lowest fluxes may be surprisingly closely associated spatially (Fig. 1). Consequently, inferences about mass transfer will be highly dependent on where samples are collected in the flow system.

Implications for Carbonate Dissolution and Precipitation

Carbon dioxide loss is classically associated with devolatilzation reactions such as: calcite + quartz = wollastonite + CO_2. More recently, it has also been recognized that stoichiometric or near stoichiometric carbonate dissolution (e.g., Frezzotti et al. 2011; Ague and Nicolescu, 2014) or precipitation (e.g., Piccoli et al. 2016; Scambelluri et al. 2016) of carbonate phases may occur. In metacarbonate rocks in which calcite or aragonite are the dominant

carbonate phase, it turns out that stoichiometric carbonate gains or losses will plot near the 1:1 line on a Ca-volatile percentage mass change diagram, facilitating distinction of volatile loss behavior.

Three types of behavior are shown on Figure 23d. A field for devolatilization is clearly evident, highlighting the important role played by this process. On the other hand, two subduction zone metacarbonate examples plot near the 1:1 mass change line and underwent extensive $CaCO_3$ dissolution (LM11, HREE8). Finally, a syn-metamorphic carbonate-bearing vein from the regional greenschist facies records $CaCO_3$ precipitation (HREE3). It is tempting to speculate that carbonate dissolved at deeper levels of the metamorphic system was redeposited at shallower levels in this vein. Going forward, the answers to these and other questions relating to CO_2 mass transfer will be critical to resolve in order to obtain a deeper understanding of deep carbon cycling in the lithosphere.

Acknowledgements

I would like to express my deep appreciation to my colleagues D.M. Rye and M.T. Brandon for countless discussions of fluid-driven processes here at Yale; to J.M. Ferry and D. Rumble for unique geological field experiences that greatly expanded my thinking about metamorphism; to undergraduate students, graduate students, and postdocs J.A. Axler, E.F. Baxter, C.M. Breeding, C.E. Bucholz, C.J. Carson, X. Chu, E.L. Donald, S. Emmanuel, K. Karsh, D.S. Keller, T. Lyubetskaya, R.L. Masters, F. Piccoli, E.M. Stewart, M. Tian, and J.L.M. van Haren who have worked on fluid-rock interaction problems in the lab; and to collaborators and coauthors throughout the years. I sincerely thank J.M. Ferry, R. Milke, and T. Müller for their invitation contribute to this special volume, and S. Chakraborty and S.C. Penniston-Dorland

for thorough and constructive reviews that significantly improved the paper. Financial support from the National Science Foundation (particularly EAR- EAR-0105927, 0509934, 0744154, 0948092, and 1250269), the Department of Energy (DE-FE0004375), the Deep Carbon Observatory, and Yale University is gratefully acknowledged. This report was prepared as an account of work sponsored by an agency of the United States Government. Neither the United States Government nor any agency thereof, nor any of their employees, makes any warranty, express or implied, or assumes any legal liability or responsibility for the accuracy, completeness, or usefulness of any information, apparatus, product, or process disclosed, or represents that its use would not infringe privately owned rights. Reference herein to any specific commercial product, process, or service by trade name, trademark, manufacturer, or otherwise does not necessarily constitute or imply its endorsement, recommendation, or favoring by the United States Government or any agency thereof. The views and opinions of authors expressed herein do not necessarily state or reflect those of the United States Government or any agency thereof.

Appendix

The following is a brief summary of the mass balance equations describing the chemical and volumetric changes of metasomatism. The reader is referred to Gresens (1967), Grant (1986), Brimhall and Dietrich (1987), Brimhall et al. (1988), Ague (1994a), Baumgartner and Olsen (1995), Ague and van Haren (1996), Ague (2011), and Durand et al. (2015) for discussion of various aspects of these equations. The mass change of a mobile constituent can be calculated using equation (6) for a general system with specified geochemical reference frame, equation (10) for a constant volume system, or equation (16) for a constant mass system.

General System

827 The basic mass balance expression relevant for describing chemical changes in rocks is
828 (e.g., Brimhall et al. 1988; Ague, 1994a):

829 $$V^0 \rho^0 C_i^0 = V' \rho' C_i', \qquad (1)$$

830 in which V and ρ are rock volume and density respectively (including pore space), C_i is the
831 concentration of a reference (immobile) species i defining the geochemical reference frame
832 (mass units), and the ^{0} and $^/$ superscripts refer to the initial and final (altered) states. The volume
833 strain ε is given by:

834 $$\varepsilon = \frac{V' - V^0}{V^0}. \qquad (2)$$

835 Substitution of equation (2) into equation (1) and rearranging for volume strain yields:

836 $$\varepsilon_i = \left(\frac{C_i^0}{C_i'}\right)\left(\frac{\rho^0}{\rho'}\right) - 1, \qquad (3)$$

837 in which ε_i denotes that strain is being computed on the basis of reference element i. The
838 fractional change in mass for some mobile constituent j (τ^j) is given by:

839 $$\tau^j = \frac{V'\rho' C_j' - V^0 \rho^0 C_j^0}{V^0 \rho^0 C_j^0} = \frac{V'\rho' C_j'}{V^0 \rho^0 C_j^0} - 1. \qquad (4)$$

840 Noting that $\varepsilon_i + 1 = V'/V^0$, substitution yields:

841 $$\tau_i^j = \frac{\rho'}{\rho^0}\frac{C_j'}{C_j^0}(\varepsilon_i + 1) - 1, \qquad (5)$$

842 providing a quantitative relationship between changes in rock chemical and physical properties.
843 This expression may be simplified further by substituting explicitly for volume change:

844 $$\tau_i^j = \left(\frac{C_i^0}{C_i'}\right)\left(\frac{C_j'}{C_j^0}\right) - 1. \qquad (6)$$

845 The total change in rock mass T^{rm} is:

$$T^{rm} = \frac{V'\rho' - V^0\rho^0}{V^0\rho^0} = \frac{V'\rho'}{V^0\rho^0} - 1. \qquad (7)$$

From equation (1), the right side of equation (7) can be recast to give:

$$T_i^{rm} = \left(\frac{C_i^0}{C_i'}\right) - 1. \qquad (8)$$

Equations (3), (6), and (8) give fractional changes; percentage changes are obtained by multiplying by 100 (gains are positive, losses negative).

Constant Volume or Known Volume Change System

For a system with no volume change, the basic mass balance of equation (1) simplifies to:

$$\rho^0 C_i^0 = \rho' C_i'. \qquad (9)$$

The mass change for a mobile constituent *j* is easily obtained from equation (5) by setting the volume strain to zero:

$$\tau_i^j = \frac{\rho'}{\rho^0}\frac{C_j'}{C_j^0} - 1. \qquad (10)$$

As final and initial volumes are equal, the total rock mass change in a constant volume system is controlled by the density ratio:

$$T^{rm} = \frac{V'\rho' - V^0\rho^0}{V^0\rho^0} = \frac{\rho'}{\rho^0} - 1. \qquad (11)$$

If the volume change is non-zero, but known, then the change in mass of a mobile constituent *j* can be calculated from equation (5) by substituting in the known value of volume strain. To calculate the total mass change, we begin by rearranging equation (2):

$$V' = \varepsilon V^0 + V^0. \qquad (12)$$

Substituting this expression for V' into equation (7) and rearranging gives the expression for the total mass change in a system with known, non-zero volume change:

866 $$T^{rm} = \frac{(\varepsilon + 1)\rho' - \rho^0}{\rho^0}. \qquad (13)$$

867 If the volume change is zero, this expression reduces to equation (11).

868 **Constant Mass or Known Mass Change System**

869 In systems with no overall rock mass change, the concentrations of a reference species in

870 the initial and final states are equal. Thus, equation (1) simplifies to:

871 $$V^0\rho^0 = V'\rho'. \qquad (14)$$

872 It follows that the volume strain expression of equation (3) can be written as follows for a

873 constant mass system:

874 $$\varepsilon = \frac{\rho^0}{\rho'} - 1. \qquad (15)$$

875 Rearranging this expression to give $\varepsilon + 1$ and then substituting the equivalent density ratio into

876 equation (5) yields the mass change for mobile constituent *j*:

877 $$\tau^j = \frac{C'_j}{C^0_j} - 1. \qquad (16)$$

878 As there is no overall rock mass change, $T^{rm} = 0$.

879 In constant mass systems, 1 kg of initial rock has the same mass of 1 kg after alteration.

880 Note, however, that considerable changes in the masses of *individual* elements may have taken

881 place. The requirement is that the amount of mass lost must equal the amount gained, in order to

882 keep the overall mass constant.

883 If the total change in rock mass T^{rm} is non-zero, but known, then equation (8) for the total

884 rock mass change can be rearranged and substituted into equation (3) for volume strain to yield:

885 $$\varepsilon = \frac{\rho^0}{\rho'}\left(T^{rm} + 1\right) - 1. \qquad (17)$$

Similarly, substitution of equation (8) into equation (6) yields the following expression for the mass change of a mobile constituent in a system with known overall mass change T^{rm}:

$$\tau^j = \left(\frac{C'_j}{C^0_j}\right)\left(T^{rm} + 1\right) - 1 . \qquad (18)$$

References Cited

Ague, J.J. (1994a) Mass transfer during Barrovian metamorphism of pelites, south-central Connecticut, I: Evidence for composition and volume change. American Journal of Science, 294, 989-1057.

Ague, J.J. (1994b) Mass transfer during Barrovian metamorphism of pelites, south-central Connecticut, II: Channelized fluid flow and the growth of staurolite and kyanite. American Journal of Science, 294, 1061-1134.

Ague, J.J. and van Haren, J.L.M. (1996) Assessing metasomatic mass and volume changes using the bootstrap, with application to deep-crustal hydrothermal alteration of marble. Economic Geology, 91, 1169-1182.

Ague, J.J. (1997) Crustal mass transfer and index mineral growth in Barrow's garnet zone, Northeast Scotland. Geology, 25, 73-76.

Ague, J. J. (2003) Fluid infiltration and transport or major, minor, and trace elements during regional metamorphism of carbonate rocks, Wepawaug Schist, Connecticut, USA. American Journal of Science, 303, 753-816.

Ague J.J. and Baxter, E.F. (2007) Brief thermal pulses during mountain building recorded by Sr diffusion in apatite and multicomponent diffusion in garnet. Earth and Planetary Science Letters, 261, 500-516.

Ague, J.J. (2011) Extreme channelization of fluid and the problem of element mobility during Barrovian metamorphism. American Mineralogist, 96, 333-352.

909 Ague, J.J. (2014) Fluid Flow in the Deep Crust. In Treatise on Geochemistry (eds. H.D. Holland
910 and K.K. Turekian), 2nd Edition, vol 4, Elsevier, Oxford, p. 203-247.
911 Ague, J.J., and Nicolescu, S. (2014) Carbon dioxide released from subduction zones by fluid-
912 mediated reactions. Nature Geoscience, 7, 355-360.
913 Aitchison, J. (1986) The statistical analysis of compositional data. London, Chapman and Hall,
914 416 p.
915 Bailey, E.H. and Ragnarsdottir, K.V. (1994) Uranium and thorium solubilities in subduction
916 zone fluids. Earth and Planetary Science Letters, 124, 119-129.
917 Bali, E., Audétat, A., and Keppler, H. (2011) The mobility of U and Th in subduction zone
918 fluids: an indicator of oxygen fugacity and fluid salinity. Contributions to Mineralogy
919 and Petrology, 161, 597-613.
920 Banner, J.L. and Hanson, G.N. (1990) Calculation of simultaneous isotopic and trace element
921 variations during water-rock interaction with applications to carbonate diagenesis.
922 Geochimica et Cosmochimica Acta, 54, 3123-3137.
923 Bao, S.-X., Zhou, H.-Y., Peng, X.-T., Ji, F.-W., and Yao, H.-Q. (2008) Geochemistry of REE
924 and yttrium in hydrothermal fluids from the Endeavour segment, Juan de Fuca Ridge.
925 Geochemical Journal, 42, 359-370.
926 Barrow, G. 1893. On an intrusion of muscovite-biotite gneiss in the south-eastern highlands of
927 Scotland, and its accompanying metamorphism. Quarterly Journal of the Geological
928 Society of London, 49, 330-354.
929 Barrow, G. 1912. On the geology of the lower Dee-side and the southern highland border.
930 Proceedings of the Geologist's Association, 23, 149-156.

Bartley, J.M. (1986) Evaluation of REE mobility in low-grade metabasalts using mass-balance calculations. Norsk Geologisk Tidsskrift, 66, 145-152.

Battles, D.A. and Barton, M.D. (1995) Arc-related sodic hydrothermal alteration in the western United States. Geology, 23, 913-916.

Bau, M. (1991) Rare-earth element mobility during hydrothermal and metamorphic fluid-rock interaction and the significance of the oxidation state of europium. Chemical Geology, 93, 219-230.

Baumgartner, L. P. and Olsen, S. N. (1995) A least-squares approach to mass transport calculations using the isocon method. Economic Geology, 90, 1261-1270.

Baxter, E.F. and Scherer, E.E. (2013) Garnet geochronology: timekeeper of tectonometamorphic processes. Elements, 9, 433-438.

Bebout, G. E. and Barton, M. D. (2002) Tectonic and metasomatic mixing in a high-T, subduction-zone mélange – insights into the geochemical evolution of the slab-mantle interface. Chemical Geology, 187, 79-106.

Bebout, G.E. (2016) Chemical and isotopic cycling in subduction zones (eds. H.D. Holland and K.K. Turekian), 2nd Edition, vol 4, Elsevier, Oxford, p. 703-747.

Bebout, G.E. and Penniston-Dorland, S. (2016) Fluid and Mass Transfer at Subduction Interfaces—The Field Metamorphic Record. Lithos, doi: 10.1016/j.lithos.2015.10.007.

Becker, H., Jochum, K.P., and Carlson, R.W. (2000) Trace element fractionation during dehydration of eclogites from high-pressure terranes and the implications for element fluxes in subduction zones. Chemical Geology, 163, 65–99.

952 Beinlich, A., Klemd, R., John, T., and Gao, J. (2010) Trace-element mobilization during Ca-
953 metasomatism along a major fluid conduit: Eclogitization of blueschist as a consequence
954 of fluid–rock interaction. Geochimica et Cosmochimica Acta, 74, 1892-1922.
955 Bickle, M.J. (1996) Metamorphic decarbonation, silicate weathering and the long-term carbon
956 cycle. Terra Nova, 8, 270-276.
957 Boehnke, P., Watson, E.B., Trail, D., Harrison, T.M., Schmitt, A.K. (2013) Zircon saturation re-
958 revisited. Chemical Geology, 324-334.
959 Breeding C. M. and Ague J. J. (2002) Slab-derived fluids and quartz-vein formation in an
960 accretionary prism, Otago Schist, New Zealand. Geology, 30, 499-502.
961 Breeding, C. M., Ague, J. J., and Bröcker, M. (2002) Fluid mass transfer of trace elements during
962 retrogression of a high pressure, low temperature metamorphic terrane, Tinos and Syros
963 Islands, Cyclades, Greece. Geological Society of America Abstracts with Programs, 34,
964 503.
965 Breeding, C.M., Ague, J.J., Bröcker, M., and Bolton, E. W. (2003) Blueschist preservation in a
966 retrograded, high-pressure, low-temperature metamorphic terrane, Tinos, Greece:
967 Implications for fluid flow paths in subduction zones. Geochemistry, Geophysics,
968 Geosystems, 4, DOI: 10.1029/2002GC000380.
969 Breeding, C. M., Ague, J. J., and Bröcker, M. (2004) Fluid-metasedimentary rock interactions
970 and the chemical composition of arc magmas. Geology, 32, 1041-1044.
971 Brimhall, G.H. (1977) Early fracture-controlled disseminated mineralization at Butte, Montana.
972 Economic Geology, 72, 37-59.
973 Brimhall, G.H and Dietrich, W.E. (1987) Constitutive mass balance relations between chemical
974 composition, volume, density, porosity, and strain in metasomatic hydrochemical

975 systems: Results on weathering and pedogenesis. Geochimica et Cosmochimica Acta, 51,
976 567-587.
977 Brimhall, G.H, Lewis, C.J., Ague, J.J., Dietrich, W.E., Hampel, J., Teague, T., and Rix, Peter
978 (1988) Metal enrichment in bauxites by deposition of chemically mature aeolian dust.
979 Nature, 333, 819-824.
980 Bucholz, C.E. and Ague, J.J. (2010) Fluid flow and Al transport during quartz-kyanite vein
981 formation, Unst, Shetland Islands, Scotland. Journal of Metamorphic Geology, 28, 19-39.
982 Carson, C.J. and Ague, J.J. (2008) Early-Palaeozoic metasomatism of the Archaean Napier
983 Complex, East Antarctica: Geological Society, London, Special Publications 2008, 308,
984 283-316, doi:10.1144/SP308.14.
985 Centrella, S., Austrheim, H., and Putnis, A. (2016) Mass transfer and trace element redistribution
986 during hydration of granulites in the Bergen Arcs, Norway. Lithos, 262, 1-10.Chayes, F.
987 (1949) On correlation in petrology. Journal of Geology, 57, 239-254.
988 Chayes, F. (1971) Ratio Correlation. University of Chicago Press, Chicago, 99 p.
989 Chowdhury, P., Taludar, M., Sengupta, P., Sanyal, S., and Mukopadhyay, D. (2013) Controls of
990 P-T path and element mobility on the formation of corundum pseudomorphs in
991 Paleoproterozoic high-pressure anorthosite from Sittampundi, Tamil Nadu, India.
992 American Mineralogist, 98, 1725-1737.
993 Connolly, J.A.D. and Podladchikov, Y.Y. (2007) Decompaction weakening and channeling
994 instability in ductile porous media: Implications for asthenospheric melt segregation.
995 Journal of Geophysical Research-Solid Earth, 112, doi:10.1029/2005JB004213.

Dasgupta, S., Chakraborty, S., and Neogi, S. (2009) Petrology of an inverted Barrovian sequence of metapelites in Sikkim Himalaya, India: constraints on the tectonics of inversion. American Journal of Science, 309, 43-84.

De Jong, G. and Williams, P.J. (1995) Giant metasomatic system formed during exhumation of mid-crustal Proterozoic rocks in the vicinity of the Cloncurry Fault, northwest Queensland. Australian Journal of Earth Sciences, 42, 281-290.

Dipple, G.M. and Ferry, J.M. (1992) Metasomatism and fluid flow in ductile fault zones. Contributions to Mineralogy and Petrology, 112, 149–164.

Dostal, J., Strong, D.F., and Jamieson, R.A. (1980) Trace element mobility in the mylonite zone within the ophiolite aureole, St. Anothony Complex, Newfoundland. Earth and Planetary Science Letters, 49, 188-192.

Durand, C., Oliot, E., Marquer, D., Sizun, J-P (2015) Chemical mass transfer in shear zones and metacarbonate xenoliths: a comparison of four mass balance approaches. European Journal of Mineralogy, 27, 731-754.

Faccenda, M, Gerya, T., and Burlini, L. (2009) Deep slab hydration induced by bending-related variations in tectonic pressure. Nature Geoscience, 2, 790-793.

Ferrando, S., Frezzotti, M.L., Dallai, L. and Compagnoni, R. (2005) Multiphase solid inclusions in UHP rocks (Su-Lu, China): Remnants of supercritical silicate-rich aqueous fluids released during continental subduction. Chemical Geology, 223, 68-81.

Ferry J. M. (1992) Regional metamorphism of the Waits River Formation, eastern Vermont: Delineation of a new type of giant metamorphic hydrothermal system. Journal of Petrology, 33, 45-94.

1018 Ferry, J.M. (1994) Overview of the petrological record of fluid flow during regional
1019 metamorphism in northern New England. American Journa1 of Science, 294, 905-988.
1020 Ferry, J.M. and Dipple, G.M. (1991) Fluid flow, mineral reactions, and metasomatism. Geology,
1021 19, 211-214.
1022 Floess, D., Baumgartner, L.P., and Vonlanthen, P. (2015) An observational and thermodynamic
1023 investigation of carbonate partial melting. Earth and Planetary Science Letters, 409, 147-
1024 156.
1025 Frezzotti, M.L., Selverstone, J., Sharp, Z.D., and Compagnoni, R. (2011) Carbonate dissolution
1026 during subduction revealed by diamond-bearing rocks from the Alps. Nature Geoscience,
1027 4, 703-706.
1028 Galvez, M., Martinez, I., Beyssac, O., Benzerara, K., Agrinier, P., and Assayag, N. (2013)
1029 Metasomatism and graphite formation at a lithological interface in Malaspina (Alpine
1030 Corsica, France). Contributions to Mineralogy and Petrology, 166, 1687-1708.
1031 Gammons, C.H., Wood, S.A., and Williams-Jones, A.E. (1996) The aqueous geochemistry of the
1032 rare earth elements and yttrium: VI. Stability of neodymium chloride complexes from 25
1033 to 300°C. Geochimica et Cosmochimica Acta, 23, 4615-4630.
1034 Gao, J., John, T., Klemd, R., and Xiong, X. (2007) Mobilization of Ti-Nb-Ta during subduction:
1035 Evidence from rutile-bearing dehydration segregations and veins hosted in eclogite,
1036 Tianshan, NW China. Geochimica et Cosmochimica Acta, 71, 4974–4996.
1037 Gieré, R. (1990) Hydrothermal mobility of Ti, Zr and REE: examples from the Bergell and
1038 Adamello contact aureoles (Italy). Terra Nova, 2, 60–67.
1039 Grant, J.A. (1986) The isocon diagram—A simple solution to Gresens' equation for metasomatic
1040 alteration. Economic Geology, 81, 1976-1982.

1041 Gruau, G., Tourpin, S., Fourcade, S., and Blais, S. (1992) Loss of isotopic (Nd, O) and chemical
1042 (REE) memory during metamorphism of komatiites: new evidence from eastern Finland.
1043 Contributions to Mineralogy and Petrology, 112, 66-82.
1044 Gresens R.L. (1967) Composition-volume relations of metasomatism. Chemical Geology, 2, 47-
1045 65.
1046 Griffin, W.L. and Breuckner, H.K. (1985) REE, Rb-Sr, and Sm-Nd studies of Norwegian
1047 eclogites. Chemical Geology, 52, 249-271.
1048 Hanson, R.B. (1997) Hydrodynamics of regional metamorphism due to continental collision.
1049 Economic Geology, 92, 880-891.
1050 Hansen, E.C. and Harlov, D.E. (2007) Whole-rock, phosphate, and silicate compositional trends
1051 across an amphibolite- to granulite-facies transition,Tamil Nadu, India. Journal of
1052 Petrology, 48, 1641-1680.
1053 Harlov, D.E. (2012) The potential role of fluids during regional granulite facies dehydration in
1054 the lower crust. Goescience Frontiers, 3, 813-827.
1055 Harlov, D.E., Wirth, R., and Hetherington, C.J. (2011) Fluid-mediated partial alteration in
1056 monazite: the role of coupled dissolution–reprecipitation in element redistribution and
1057 mass transfer. Contributions to Mineralogy and Petrology, 162, 329-348.
1058 Harlov, D.E. (2012) The potential role of fluids during regional granulite facies dehydration in
1059 the lower crust. Geoscience Frontiers, 3, 813-827.
1060 Hellman, P.L., Smith, R.E., and Henderson, P. (1979) The mobility of the rare earth elements:
1061 Evidence and implications from selected terrains affected by burial metamorphism.
1062 Contributions to Mineralogy and Petrology, 71, 23-44.

Hermann, J., 2002, Allanite: thorium and light rare earth element carrier in subducted crust: Chemical Geology, 192, 289-306.

Hermann, J. and Spandler, C.J. (2008) Sediment melts at sub-arc depths: an experimental study. Journal of Petrology, 49, 717-740.

Hermann, J., Zheng, Y., and Rubatto, D. (2013) Deep fluids in subducted continental crust. Elements, 9, 281-287.

John, T., Klemd, R., Gao, J., Garbe-Schönberg, C-.D. (2008) Trace-element mobilization in slabs due to non steady-state fluid–rock interaction: Constraints from an eclogite-facies transport vein in blueschist (Tianshan, China). Lithos, 103, 1-24.

Johnson, M.C. and Plank, T. (1999) Dehydration and melting experiments constrain the fate of subducted sediments. Geochemistry, Geophysics, and Geosystems, v. 1, doi: 10.1029/1999GC000014.

Kelsey, D.E., and Powell, R. (2011) Progress in linking accessory mineral growth and breakdown to major mineral evolution in metamorphic rocks: a thermodynamic approach in the Na_2O-CaO-K_2O-FeO-MgO-Al_2O_3-SiO_2-H_2O-TiO_2-ZrO_2 system. Journal of Metamorphic Geology, 29, 151-166.

Long, K.R., Van Gosen, B.S., Foley, N.K., and Cordier, D. (2010) The principal rare earth elements deposits of the United States—A summary of domestic deposits and a global perspective. U.S. Geological Survey, Scientific Investigations Report 2010-5220, 96 p.

Lee, J.H. and Byrne, R.H. (1992) Examination of comparative rare earth element complexation behavior using linear free-energy relationships. Geochimica et Cosmochimica Acta, 56, 1127-l 137.

Lyubetskaya, T. and Ague, J.J. (2009) Modeling the magnitudes and directions of regional metamorphic fluid flow in collisional orogens. Journal of Petrology, 50, 1505-1531.

Manning, C.E. (2004). The chemistry of subduction-zone fluids. Earth and Planetary Science Letters, 223, 1-16.

Manning, C.E. and Aranovich, L.Y. (2014) Brines at high pressure and temperature: Thermodynamic, petrologic and geochemical effects. Precambrian Research, 253, 6-16.

Marsh, J.H., Grew, E.S., Gerbi, C.C., and Yates, M.G. (2012) The petrogenesis of the garnet menzerite-(Y) in granulite facies rocks of the Parry Sound Domain, Grenville Province, Ontario. The Canadian Mineralogist, 50, 73-99.

Masters, R.L. and Ague, J.J. (2005) Regional-scale fluid flow and element mobility in Barrow's metamorphic zones, Stonehaven, Scotland. Contributions to Mineralogy and Petrology, 150, 1-18.

Meschede, M. (1986) A method of discriminating between different types of mid-ocean ridge basalts and continental tholeiites with the Nb-Zr-Y diagram. Chemical Geology, 56, 207-218.

Melzer, S. and Wunder, B. (2000) Island-arc basalt alkali ratios: Constraints from phengite-fluid partitioning experiments: Geology, 28, 583–586.

Michard, A. and Albarède, F. (1986) The REE content of some hydrothermal fluids. Chemical Geology, 55, 51-60.

Miller, D.P., Marschall, H.R., and Schumacher, J.C. (2009) Metasomatic formation and petrology of blueschist-facies hybrid rocks from Syros (Greece): Implications for reactions at the slab–mantle interface. Lithos, 107, 53-67.

Munz, I.A., Wayne, D., and Austrheim, H. (1994) Retrograde fluid infiltration in the high-grade Modum Complex, South Norway: Evidence for age, source, and REE mobility. Contributions to Mineralogy and Petrology, 116, 32-46.

Newton, R.C., Smith, J.V., and Windley, B.F. (1990) Carbonic metamorphism, granulites, and crustal growth. Nature, 288, 45-50.

Noll, P.D., Newsom, H.E., Leeman, W.P., and Ryan, J.G. (1996) The role of hydrothermal fluids in the production of subduction zone magmas: Evidence from siderophile and chalcophile trace elements and boron. Geochimica et Cosmochimica Acta, 60, 587–611.

Norton, D.L. and Knapp, R. (1977) Transport phenomena in hydrothermal systems: The nature of porosity. American Journal of Science, 277, 913-936.

Oliver, N.H.S. (1996) Review and classification of structural controls on fluid flow during regional metamorphism. Journal of Metamorphic Geology, 14, 477–492.

O'Neil, J., Carlson, R.W., Paquette, J.-L., and Francis, D. (2012) Formation age and metamorphic history of the Nuvvuagittuq Greenstone Belt. Precambrian Research, 220-221, 23-44.

Pan, Y. and Fleet, M.A. (1996) Rare earth element mobility during prograde granulite facies metamorphism: significance of fluorine. Contributions to Mineralogy and Petrology, 123, 251-262.

Pearce, J.A. and Cann, J.R. (1973) Tectonic setting of mafic volcanic rocks determined using trace element analyses. Earth and Planetary Science Letters, 19, 290-300.

Pearce, J.A., Harris, N.B.W., Tindle, A.G. (1984) Trace element discrimination diagrams for the tectonic interpretation of granitic rocks. Journal of Petrology, 25, 956-983.

1129 Pearce, J.A. (1996) A user's guide to basalt discrimination diagrams (Wyman, D.A., ed.) Trace
1130 element geochemistry of volcanic rocks: Applications for massive sulfide exploration.
1131 Geological Society of Canada, Short Couse Notes, 12, 79-113.
1132 Penniston-Dorland, S.C. and Ferry, J.M. (2008) Element mobility and scale of mass transport in
1133 the formation of quartz veins during regional metamorphism of the Waits River
1134 Formation, east-central Vermont. American Mineralogist, 93, 7-21.
1135 Penniston-Dorland, S.C., Gorman, J.K., Bebout, G.E., Piccoli, P.M., and Walker, R.J. (2014)
1136 Reaction rind formation in the Catalina Schist: Deciphering a history of mechanical
1137 mixing and metasomatic alteration. Chemical Geology, 384, 47-61.
1138 Philpotts, A.R. and Ague, J.J. (2009) Principles of Igneous and Metamorphic Petrology (2nd
1139 ed.). Cambridge, Cambridge University Press, 667 p.
1140 Piccoli, F., Vitale Brovarone, A., Beyssac, O., Martinez, I., Ague, J.J., and Chaduteau, C. (2016)
1141 Carbonation by fluid-rock interactions at High-Pressure conditions: implications for
1142 carbon cycling in subduction zones. Earth and Planetary Science Letters (in press).
1143 Putnis A. and Austrheim H. (2010) Fluid induced processes: Metasomatism and metamorphism.
1144 Geofluids, 10, 254-269.
1145 Putnis A. and John T. (2010) Replacement processes in the Earth's crust. Elements, 6, 159-164.
1146 Raith, M.M., Brandt, S., Sengupta, P., Berndt, J., John, T., and Srikantappa, C. (2016) Element
1147 Mobility and Behaviour of Zircon during HT Metasomatism of Ferroan Basic Granulite
1148 at Ayyarmalai, South India: Evidence for Polyphase Neoarchaean Crustal Growth and
1149 Multiple Metamorphism in the Northeastern Madurai Province. Journal of Petrology, 57,
1150 1729-1774.

Rajesh, H.M. and Santosh, M. (2012) Charnockites and *charnockites*. Geoscience Frontiers, 3, 737-744.

Rolland, Y., Cox, S., Boullier, A-. M., Pennacchioni, G., and Mancktelow, N. (2003) Rare earth and trace element mobility in mid-crustal shear zones: insights from the Mont Blanc Massif (Western Alps). Earth and Planetary Science Letters, 214, 203-219.

Rollinson, H.R. and Windley, B.F. (1980) Selective elemental depletion during metamorphism of Archaean granulites, Scourie, NW Scotland. Contributions to Mineralogy and Petrology, 72, 257.

Rudnick, R.L., Barth, M., Horn, I., and McDonough, W.F. (2000) Rutile-bearing refractory eclogites; missing link between continents and depleted mantle. Science 287, 278–281.

Scambelluri, M., Gray E. Bebout, Belmonte, D., Gilio, M., Campomenosi, N., Collins, N., and Crispini, L. (2016) Carbonation of subduction-zone serpentinite (high-pressure ophicarbonate; Ligurian Western Alps) and implications for the deep carbon cycling. Earth and Planetary Science Letters, 441, 155-166.

Schmidt, M.W. (1996) Experimental constraints on recycling of potassium from subducted oceanic crust. Science, 272, 1927-1930.

Shaw, D.M. (1956) Geochemistry of pelitic rocks. Part III: Major elements and general geochemistry. Geological Society of America Bulletin, 67, 919-934.

Skelton A.D.L., Graham, C.M., and Bickle, M.J. (1995) Lithological and structural controls of regional 3-D fluid flow patterns during greenschist facies metamorphism of the Dalradian of the SW Scottish Highlands. Journal of Petrology, 36, 563-586.

1172 Sorensen, S.S. and Grossman, J.N. (1989) Enrichment of trace elements in garnet amphibolites
1173 from a paleo-subduction zone: Catalina Schist, southern California. Geochmica et
1174 Cosmochimica Acta, 53, 3155-3177.
1175 Spandler, C., Hermann, J., Arculus, R., Mavrogenes, J. (2003) Redistribution of trace elements
1176 during prograde metamorphism from lawsonite blueschist to eclogite facies; implications
1177 for deep subduction-zone processes. Contributions to Mineralogy and Petrology, 146,
1178 205-222.
1179 Spandler, C., Hermann, J., Arculus, R., and Mavrogenes, J. (2004) Geochemical heterogeneity
1180 and element mobility in deeply subducted oceanic crust; insights from high-pressure
1181 mafic rocks from New Caledonia. Chemical Geology, 206, 21-42.
1182 Spandler, C., Pettke, T., and Rubatto, D. (2011) Internal and external fluid sources for eclogite-
1183 facies veins in the Monviso meta-ophiolite, Western Alps: Implications for fluid flow in
1184 subduction zones. Journal of Petrology, 52, 1207–1236.
1185 Stolper, E. and Newman, S. (1994) The role of water in the petrogenesis of Mariana trough
1186 magmas. Earth and Planetary Science Letters, 121, 293–325.
1187 Stähle, H.J., Raith, M., Hoernes, S., and Delfs, A. (1987) Element mobility during incipient
1188 granulite formation at Kabbaldurga, southern India. Journal of Petrology, 28, 803-834.
1189 Tanis, E.A., Simon, A., Tschauner, O., Chow, P., Xiao, Y., Burnley, P., Cline, C.J., II, Hanchar,
1190 J.M., Pettke, T., Shen, G., and Zhao, Y. (2015) The mobility of Nb in rutile-saturated
1191 NaCl- and NaF-bearing aqueous fluids from 1–6.5 GPa and 300–800 °C. American
1192 Mineralogist, 100, 1600-1609.

1193 Taylor, S.R. and McLennan, S.M. (1985) The Continental Crust: its Composition and Evolution:
1194 an Examination of the Geochemical Record Preserved in Sedimentary Rocks. Blackwell,
1195 Oxford.
1196 Thompson, J.B. (1957) The graphical analysis of mineral assemblages in pelitic
1197 schists. American Mineralogist, 42, 842-858.
1198 Tomkins, H.S., Powell, R., and Ellis, D.J. (2007) The pressure dependence of the zirconium-in-
1199 rutile thermometer. Journal of Metamorphic Geology, 25, 703–713.
1200 Taetz, S., John, Timm, Bröcker, M., and Spandler, C., 2016, Fluid–rock interaction and
1201 evolution of a high-pressure/low-temperature vein system in eclogite from New
1202 Caledonia: insights into intraslab fluid flow processes. Contributions to Mineralogy and
1203 Petrology, 171:90, DOI 10.1007/s00410-016-1295-z.
1204 Trail, D., Watson, E.B., and Tailby, N.D. (2012) Ce and Eu anomalies in zircon as proxies for
1205 the oxidation state of magmas. Geochimica et Cosmochimica Acta, 97, 70-87.
1206 Tribuzio, R., Messiga, B., Vannucci, R., and Bottazzi, P. (1996) Rare earth element
1207 redistribution during high-pressure–low-temperature metamorphism in ophiolitic Fe-
1208 gabbros (Liguria, northwestern Italy): Implications for light REE mobility in subduction
1209 zones. Geology, 24, 711-714.
1210 Tsay, A., Zajacz, Z., and Sanchez-Valle, C. (2014) Efficient mobilization and fractionation of
1211 rare-earth elements by aqueous fluids upon slab dehydration. Earth and Planetary Science
1212 Letters, 398, 101-112.
1213 Tsay, A., Zajacz, Z., Ulmer, P., and Sanchez-Valle, C. (2016) Mobility of major and trace
1214 elements in the eclogite-fluid system and element fluxes upon slab dehydration.
1215 Geochimica et Cosmochimica Acta, in press.

1216 Turner, S., Evans, P., and Hawkesworth, C. (2001) Ultrafast source-to-surface movement of melt
1217 at island arcs from ^{226}Ra-^{230}Th systematics. Science, 292, 1363–1366.
1218 Valley J. W., Bohlen S. W., Essene E. J., and Lamb W. (1990) Metamorphism in the
1219 Adirondacks: II. The role of fluids. Journal of Petrology, 31, 555-596.
1220 van der Straaten, F., Schenk, V., John, T., and Gao, J. (2008) Blueschist-facies rehydration of
1221 eclogites (Tian Shan, NW-China): Implications for fluid–rock interaction in the
1222 subduction channel. Chemical Geology, 255, 195-219.
1223 Van Haren, J.L., Ague, J.J., and Rye, D.M. (1996) Oxygen isotope record of fluid infiltration and
1224 mass transfer during regional metamorphism of pelitic schist, Connecticut, USA.
1225 Geochimica et Cosmochimica Acta, 60, 3487-3504.
1226 Vitale Brovarone, A., Allard, O., Beyssac, O., Martin, L., and Picatto, M. (2014) Lawsonite
1227 metasomatism and trace element recycling in subduction zones. Journal of Metamorphic
1228 Geology, 32, 489-514.
1229 Wagner, T., Boyce, A.J., and Erzinger, J. (2010) Fluid-rock interaction during formation of
1230 metamorphic quartz veins: A REE and stable isotope study from the Rhenish Massif,
1231 Germany. American Journal of Science, 310, 645-682.
1232 Watson, E.B., Wark, D.A., and Thomas, J.B. (2006) Crystallization thermometers for zircon and
1233 rutile. Contributions to Mineralogy and Petrology, 151, 413–433.
1234 Watson, E.B. and Baxter, E.F. (2007) Diffusion in solid-Earth systems. Earth and Planetary
1235 Science Letters, 253, 307–327.
1236 Weaver, B.L. and Tarney, J. (1981) Chemical changes during dyke metamorphism in high-grade
1237 basement terrains. Nature, 289, 47-49.

Wickham, S.M. and Taylor, H.P. (1985) Stable isotope evidence for large-scale seawater infiltration in a regional metamorphic terrane; the Trois Seigneurs massif, Pyrenees, France. Contributions to Mineralogy and Petrology, 91, 122-137.

Wilson, C.R., Spiegelman, M., van Keken, P.E., and Hacker, B.R. (2014) Fluid flow in subduction zones: The role of solid rheology and compaction pressure. Earth and Planetary Science Letters, 401, 261-274.

Windrim, D.P., McColluch, M.T., Chappel, B.W., and Cameron, W.E. (1984) Nd isotopic systematics and chemistry of Central Australian sapphirine granulites: an example of rare earth element mobility. Earth and Planetary Science Letters, 70, 27-39.

Woronow, A., and Love, K. M. (1990) Quantifying and testing differences among means of compositional data suites. Mathematical Geology, 22, 837-852.

Yardley, B.W.D. (1986) Fluid migration and veining in the Connemara schists, Ireland, in Walther,]. V., and Wood, B. J., editors, Fluid-rock interactions during metamorphism: New York, Springer-Ver1ag, p. 109-131.

Zack, T. and John, T. (2007) An evaluation of reactive fluid flow and trace element mobility in subducting slabs. Chemical Geology, 239, 199-216.

Zack, T., Moraes, R., and Kronz, A. (2004) Temperature dependence of Zr in rutile: empirical calibration of a rutile thermometer. Contributions to Mineralogy and Petrology, 148, 471-488.

Zhao, Z.-F., Zheng, Y.-F., Chen, R.-X., Xia, Q.-X., and Wu, Y.-B. (2007) Element mobility in mafic and felsic ultrahigh-pressure metamorphic rocks during continental collision. Geochimica et Cosmochimica Acta, 71, 5244-5266.

Figure Captions

Figure 1. Fluid fluxes calculated from numerical model of flow region cut by two high permeability conduits. Flow is upward, and conduits are 100 times more permeable than matrix. Note that focusing of flow into the conduits drastically reduces fluxes in adjacent areas, such that high and low flux zones are closely associated spatially. Modified from Breeding et al. (2003; see this paper for calculation details).

Figure 2. REE concentration increase in a vein selvage system in which REE were immobile. Loss of silica from the selvage to an adjacent quartz vein caused residual enrichment of REE with no REE mass transfer into or out of the system. Data from Penniston-Dorland and Ferry (2008), site S35-1G (LM4 in Table 1).

Figure 3. Geochemical profiles illustrating changes in REE ratios due to REE mobility. **(a)** Increase in La/Lu in selvage adjacent to a quartz-rich vein cutting metapelitic rock. Increase reflects strong La gains (site 181 data from Bucholz and Ague, 2010; LREE3 in Table 1). Plus signs and circles denote least altered and more altered metacarbonate rocks, respectively. **(b)** Decrease in Eu/Sm ratio in metacarbonate rock toward veined lithologic contact. Both Eu and Sm were gained, but Sm was gained to a greater extent approaching the veined contact (site 187 data from Ague, 2003; Eu3 in Table 1). Plus signs: least altered metacarbonate rock; light green circles: diopside-zoisite metacarbonate; dark green circles: hornblende-zoisite metacarbonate; black square: vein contact zone.

Figure 4. Percentage mass change diagrams for examples that underwent little or no REE mass transfer. Note that these are not chondrite-normalized plots, but instead depict elemental percentage mass changes for altered rocks relative to their precursors (mass gains are positive, losses negative). See Table 1 for rock type descriptions.

1284 **Figure 5.** Bar code diagrams illustrating mass changes for examples that underwent little or no
1285 REE metasomatism. See Table 1 for rock type descriptions.
1286 **Figure 6.** Percentage mass change diagrams for examples that underwent LREE mass transfer.
1287 Dominant phases controlling REE mass changes are labeled (if known). LREE1 shows mass
1288 transfer for two silicified metapelite wallrock inclusions in vein. LREE3 samples 181Aii and
1289 181Aiii are 1.25 cm and 3.75 cm from vein contact, respectively. See Table 1 for rock type
1290 descriptions.
1291 **Figure 7.** Bar code diagrams illustrating mass changes for examples that underwent LREE
1292 metasomatism. See Table 1 for rock type descriptions.
1293 **Figure 8.** Percentage mass change diagrams for examples that underwent HREE mass transfer.
1294 Dominant phases controlling REE mass changes are labeled (if known). HREE3 samples 197Ai,
1295 197AS, and 197Aii are 0 cm, 1 cm, and 3 cm from vein contact, respectively. See Table 1 for
1296 rock type descriptions.
1297 **Figure 9.** Bar code diagrams illustrating mass changes for examples that underwent HREE
1298 metasomatism. See Table 1 for rock type descriptions.
1299 **Figure 10.** Percentage mass change diagrams for examples that underwent overall REE loss.
1300 Dominant phases controlling REE mass changes are labeled (if known). See Table 1 for rock
1301 type descriptions.
1302 **Figure 11.** Bar code diagrams illustrating mass changes for examples that underwent overall
1303 REE loss. See Table 1 for rock type descriptions.
1304 **Figure 12.** Percentage mass change diagrams for examples that underwent Eu mass transfer.
1305 Dominant phases controlling REE mass changes are labeled (if known). Eu3 samples 187Bii,

187Biii, and 187Mi are 2 cm, 5 cm, and 10 cm from vein contact, respectively. See Table 1 for rock type descriptions.

Figure 13. Bar code diagrams illustrating mass changes for examples that underwent Eu metasomatism. See Table 1 for rock type descriptions.

Figure 14. Percentage mass change diagrams for examples characterized by local REE redistribution. Dominant phases controlling REE mass changes are labeled (if known). Samples JTS-C (R1) and JTS-E (R2) are from blueschist-eclogite transition zone approximately 85 cm and 40 cm from vein contact, respectively (see Fig. 2 in Beinlich et al. 2010). For the shear zones cutting granitic rocks, MB69 (R3) is in the site of LREE deposition in the shear zone core, and MB71 (R4) is in the area of LREE leaching several meters away (see Fig. 6 in Rolland et al. 2003). R3 and R4 not shown on subsequent diagrams due to lack of full major element data in original paper. See Table 1 for rock type descriptions and references.

Figure 15. Mass changes for neighboring REE. Note that on this and most subsequent *x-y* plots, the scaling for negative mass changes (mass losses) has been expanded to make visualization easier. This is useful because mass losses are bounded at -100%, whereas mass gains have no set upper bound. **(a)** Ce-La. **(b)** Sm-Nd. **(c)** Eu-Sm. Examples that plot off the 1:1 trend have Eu "anomalies" relative to neighboring REE. **(d)** Lu-Yb.

Figure 16. Mass changes involving P and Y. **(a)** La-P. **(b)** REE_{max}-P. REE_{Max} denotes the maximum mass change for any REE in the rock. **(c)** Lu-P. **(d)** P-Y. **(e)** Lu-Y. **(f)** REE_{max}-Y.

Figure 17. Mass changes involving Th and U. **(a)** Th-U. **(b)** Th- REE_{max}. **(c)** U- REE_{max}. **(d)** U-Nb.

Figure 18. Mass changes involving alkalis and alkaline earths. **(a)** Na-K. Note absence of examples that gained both Na and K. **(b)** Ca-K. Note absence of examples that gained both Ca

1329 and K. **(c)** Na-Ca relations for non-subduction zone rocks. **(d)** Na-Ca relations for subduction
1330 zone rocks. **(e)** Ca-Sr. **(f)** Sr-Rb. Note rarity of coupled Sr and Rb gain, and similarity to parts (a)
1331 and (b).

1332 **Figure 19. (a)** Mass changes for Rb and K. **(b)** Mass changes for Sr and Pb.

1333 **Figure 20.** Mass changes in involving volatiles, using LOI as a proxy for volatile content. **(a)**
1334 REE_{max}-volatiles. **(b)** Na versus volatile mass changes, contoured for K mass changes. Note: (1)
1335 examples that gained K are concentrated in the field that lost Na and gained volatiles and (2) the
1336 general loss of K from all other examples.

1337 **Figure 21.** Comparison of percentage mass changes for HFSE.

1338 **Figure 22.** Examples of how HFSE mass changes could impact plotting on petrotectonic
1339 discrimination diagrams. Concentrations of Nb and Y varied to be compatible with Fig. 21. The
1340 orange ellipses illustrate mass changes of: Y±50% and Nb±25%. The green ellipses illustrate
1341 somewhat larger mass changes of: Y±75% and Nb ±50%. **(a)** Nb-Zr-Y diagram for mafic rocks
1342 (Meschede, 1986). **(b)** Nb-Y diagram for granitic rocks (Pearce et al. 1984).

1343 **Figure 23.** Mass changes for Barrovian metapelites and metacarbonate rocks from a range of
1344 settings. **(a)** Si-volatile mass changes for metapelites. Note coupled loss of silica and volatiles,
1345 illustrating dependence of silica loss on extent of devolatilization. Example that gained silica and
1346 volatiles is a silicified wallrock inclusion in a quartz vein (LREE1). **(b)** K-Rb mass changes for
1347 metapelites. Note preponderance of samples characterized by K-Rb loss. **(c)** Na-Ca mass changes
1348 for metapelites. General positive correlation due to controls on mass transfer by plagioclase
1349 feldspar. **(d)** Ca-volatile mass changes for all the metacarbonate rocks of the data set. Examples
1350 that plot close to the 1:1 line characterized by near stoichiometric dissolution or precipitation of

1351 $CaCO_3$. Tan-colored field denotes rocks that lost more CO_2 than Ca, illustrating the role of

1352 devolatilization.

1353

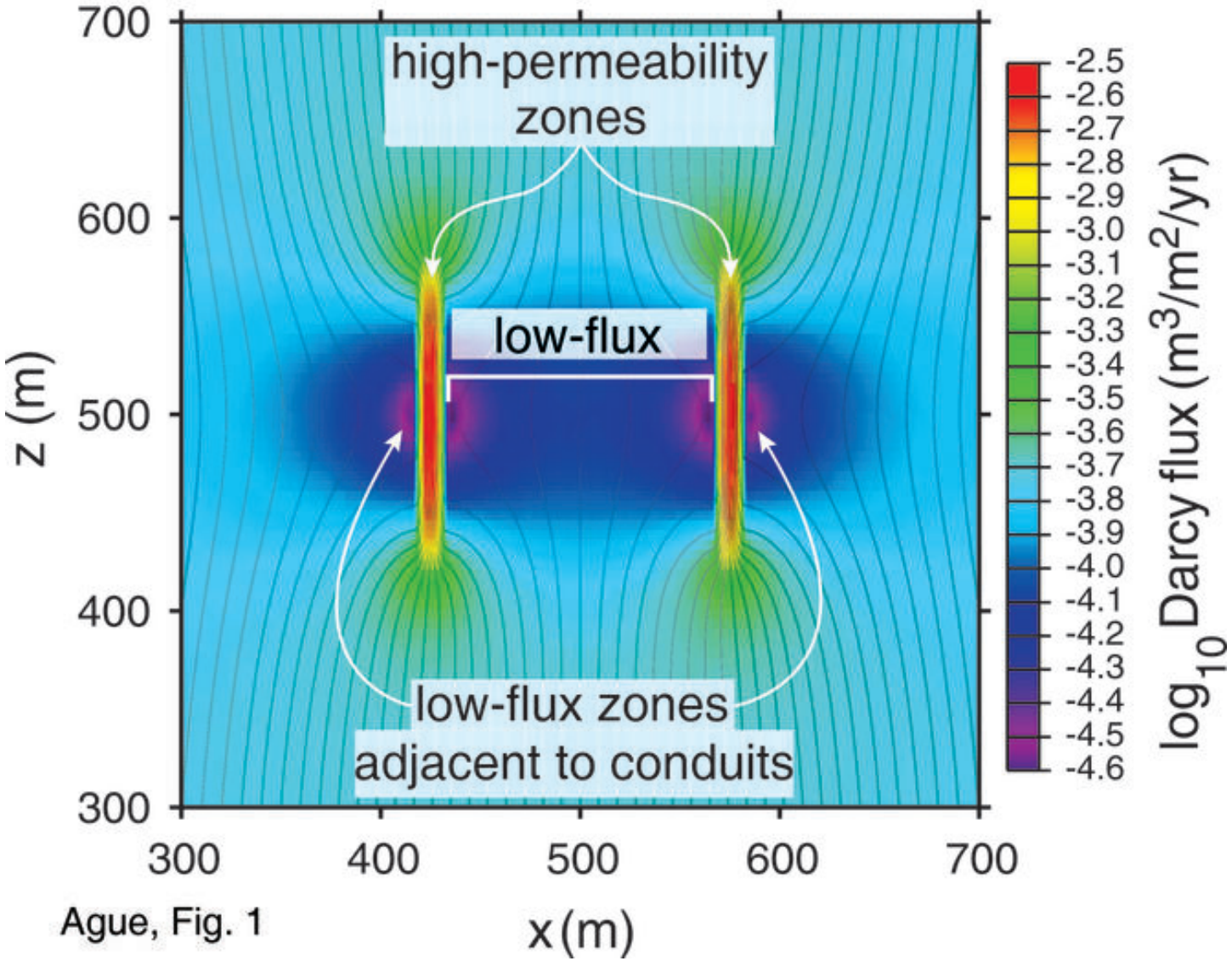

Ague, Fig. 1

This is a preprint, the final version is subject to change, of the American Mineralogist (MSA)
Cite as Authors (Year) Title. American Mineralogist, in press.
(DOI will not work until issue is live.) DOI: http://dx.doi.org/10.2138/am-2017-6130

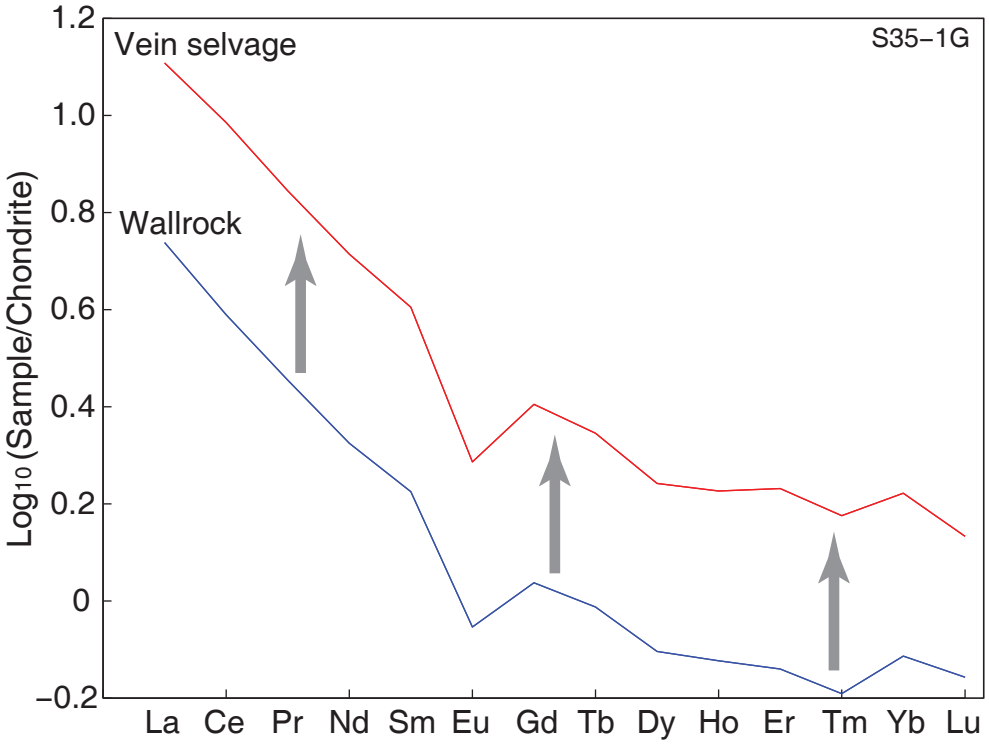

Ague, Fig. 2

This is a preprint, the final version is subject to change, of the American Mineralogist (MSA)
Cite as Authors (Year) Title. American Mineralogist, in press.
(DOI will not work until issue is live.) DOI: http://dx.doi.org/10.2138/am-2017-6130

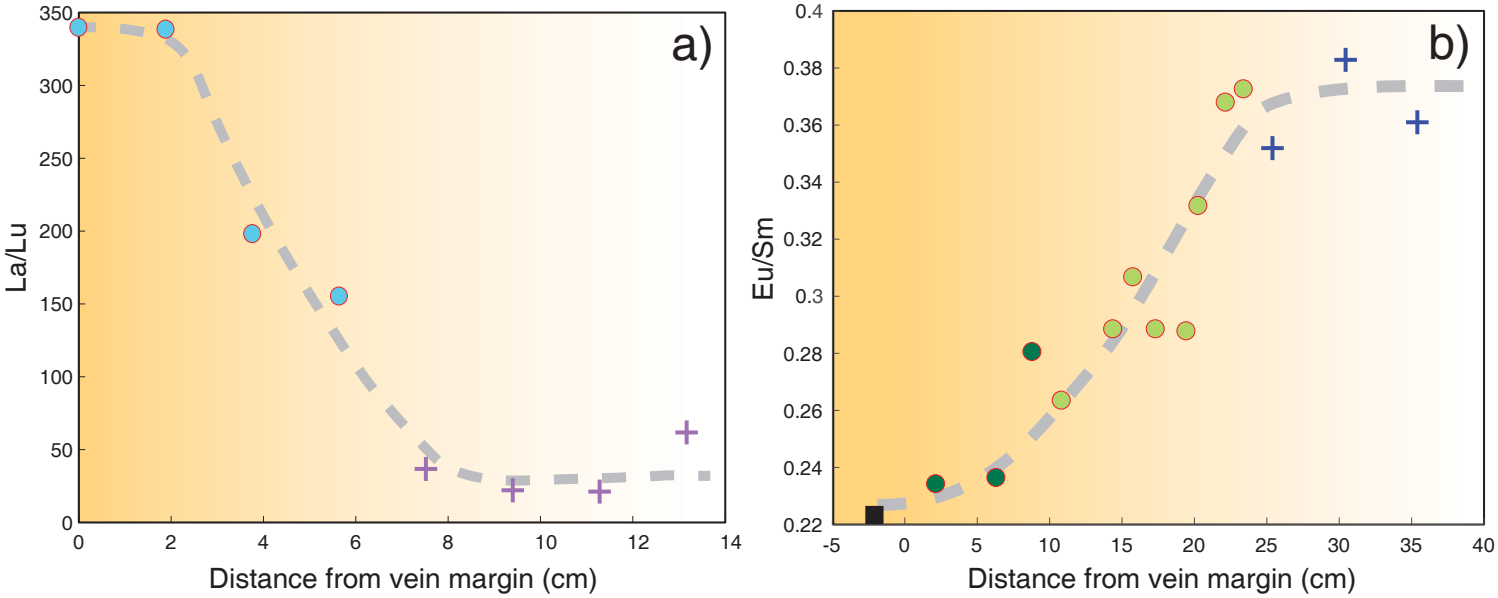

Ague, Fig. 3

This is a preprint, the final version is subject to change, of the American Mineralogist (MSA)
Cite as Authors (Year) Title. American Mineralogist, in press.
(DOI will not work until issue is live.) DOI: http://dx.doi.org/10.2138/am-2017-6130

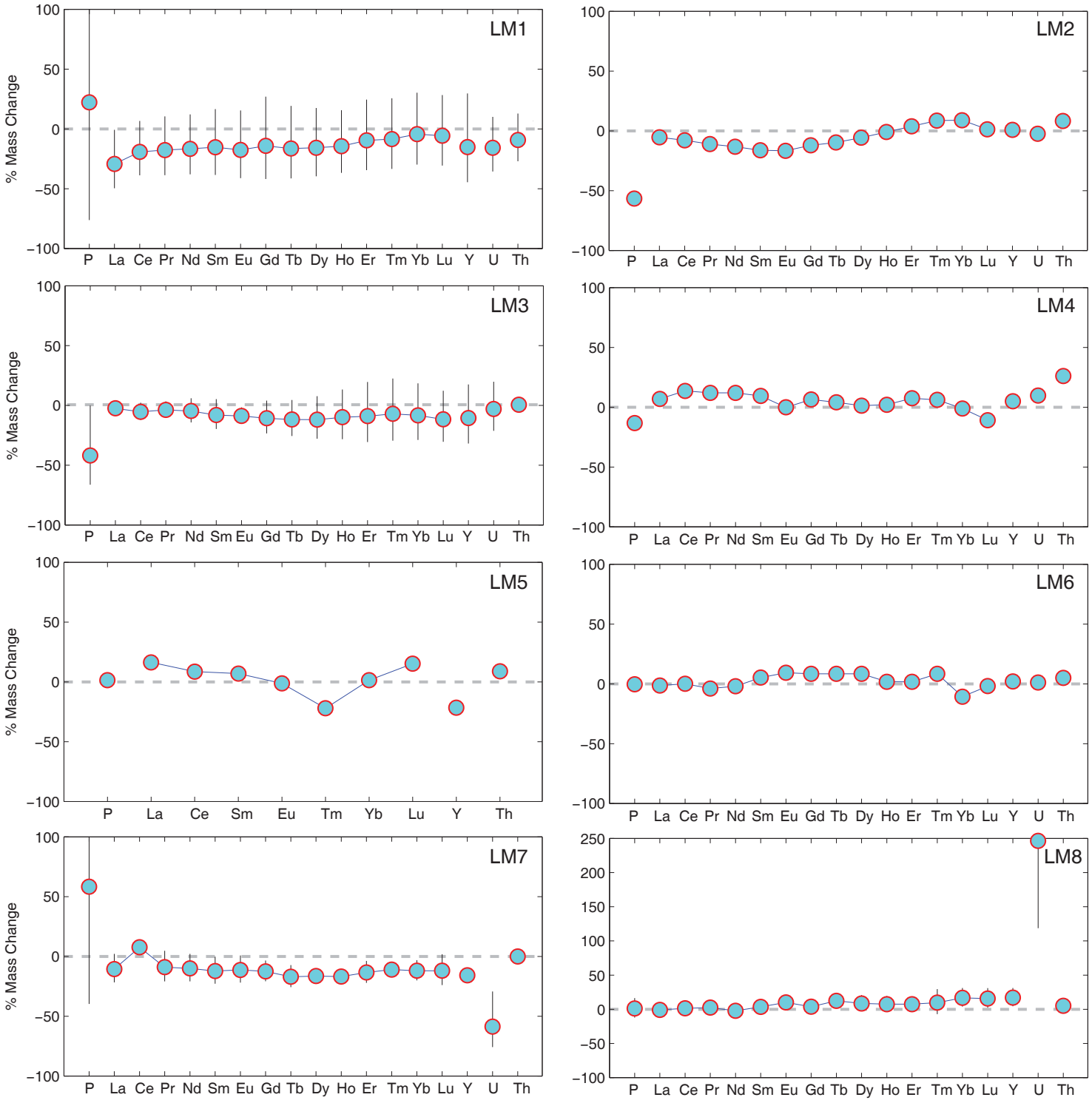

Ague, Fig. 4

This is a preprint, the final version is subject to change, of the American Mineralogist (MSA)
Cite as Authors (Year) Title. American Mineralogist, in press.
(DOI will not work until issue is live.) DOI: http://dx.doi.org/10.2138/am-2017-6130

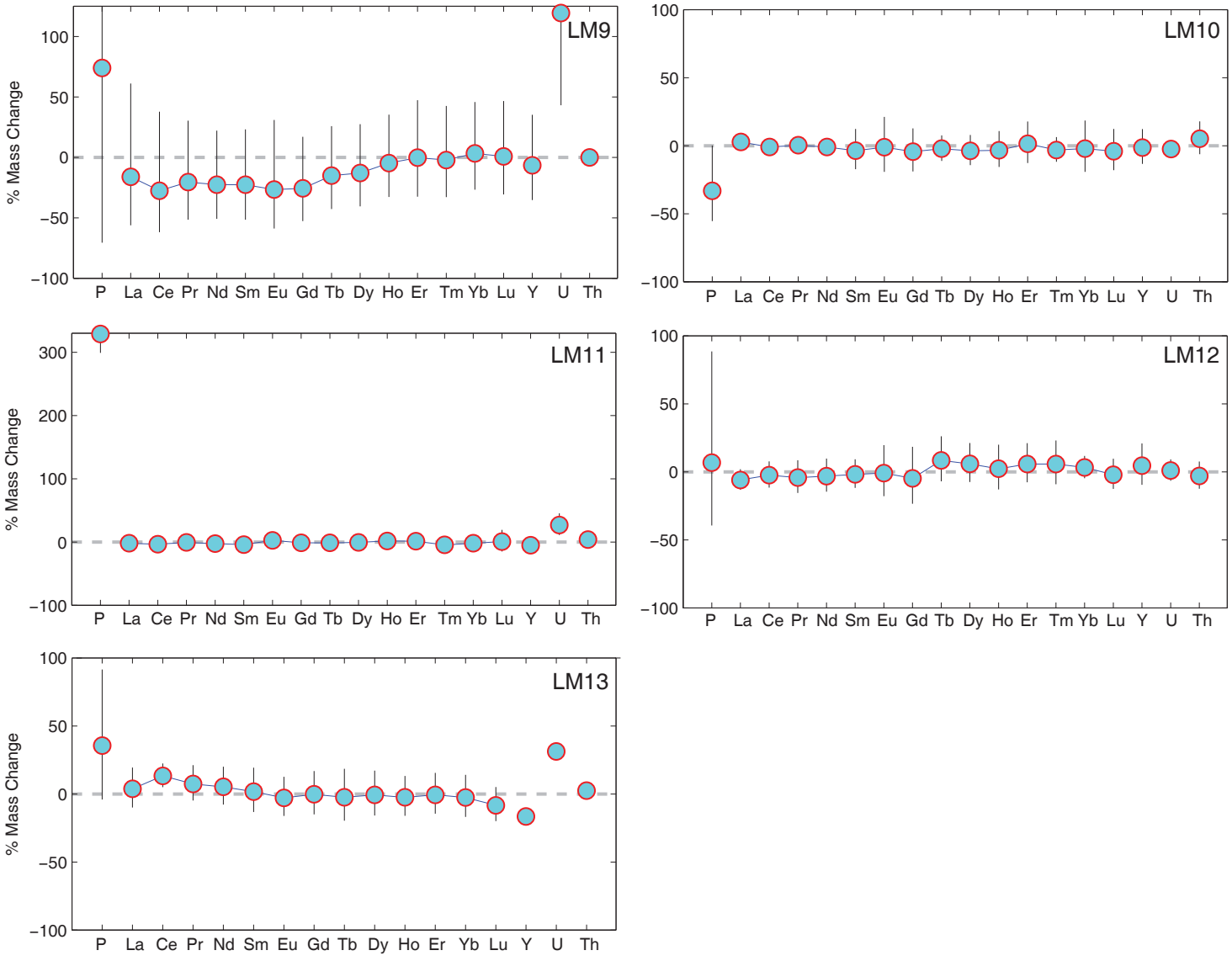

Ague, Fig. 4, continued

This is a preprint, the final version is subject to change, of the American Mineralogist (MSA)
Cite as Authors (Year) Title. American Mineralogist, in press.
(DOI will not work until issue is live.) DOI: http://dx.doi.org/10.2138/am-2017-6130

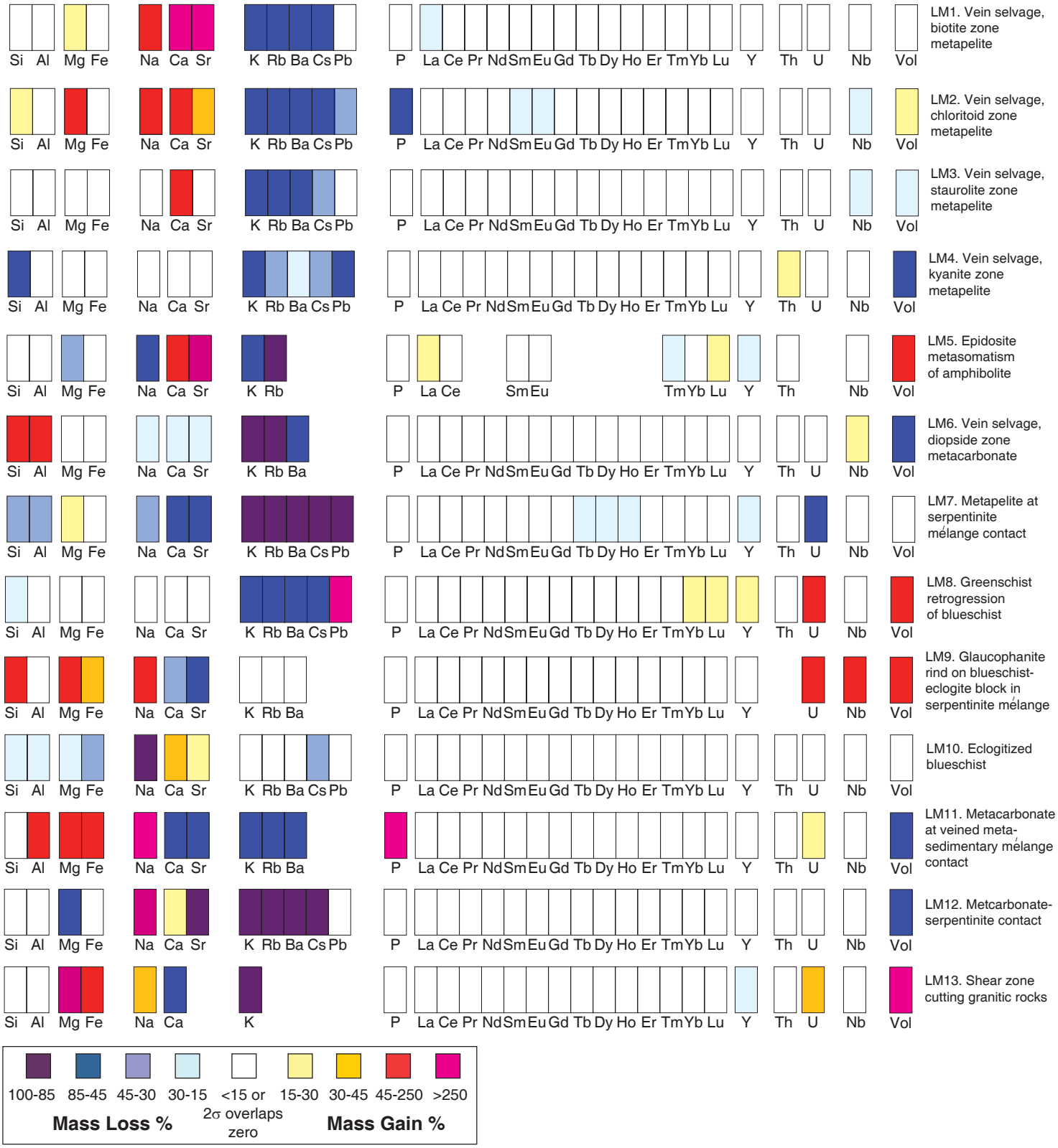

Ague, Fig. 5

This is a preprint, the final version is subject to change, of the American Mineralogist (MSA)
Cite as Authors (Year) Title. American Mineralogist, in press.
(DOI will not work until issue is live.) DOI: http://dx.doi.org/10.2138/am-2017-6130

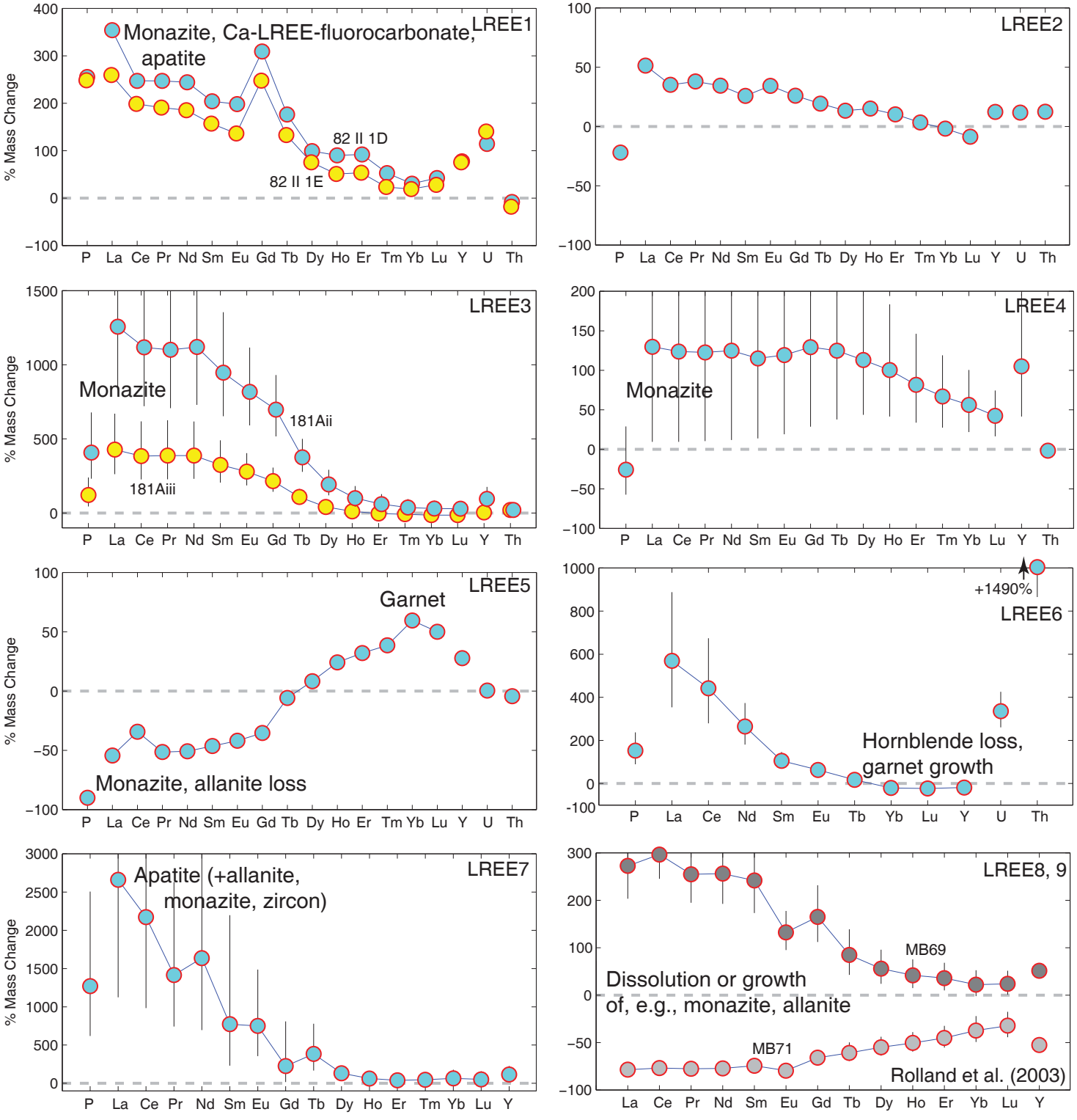

Ague, Fig. 6

This is a preprint, the final version is subject to change, of the American Mineralogist (MSA)
Cite as Authors (Year) Title. American Mineralogist, in press.
(DOI will not work until issue is live.) DOI: http://dx.doi.org/10.2138/am-2017-6130

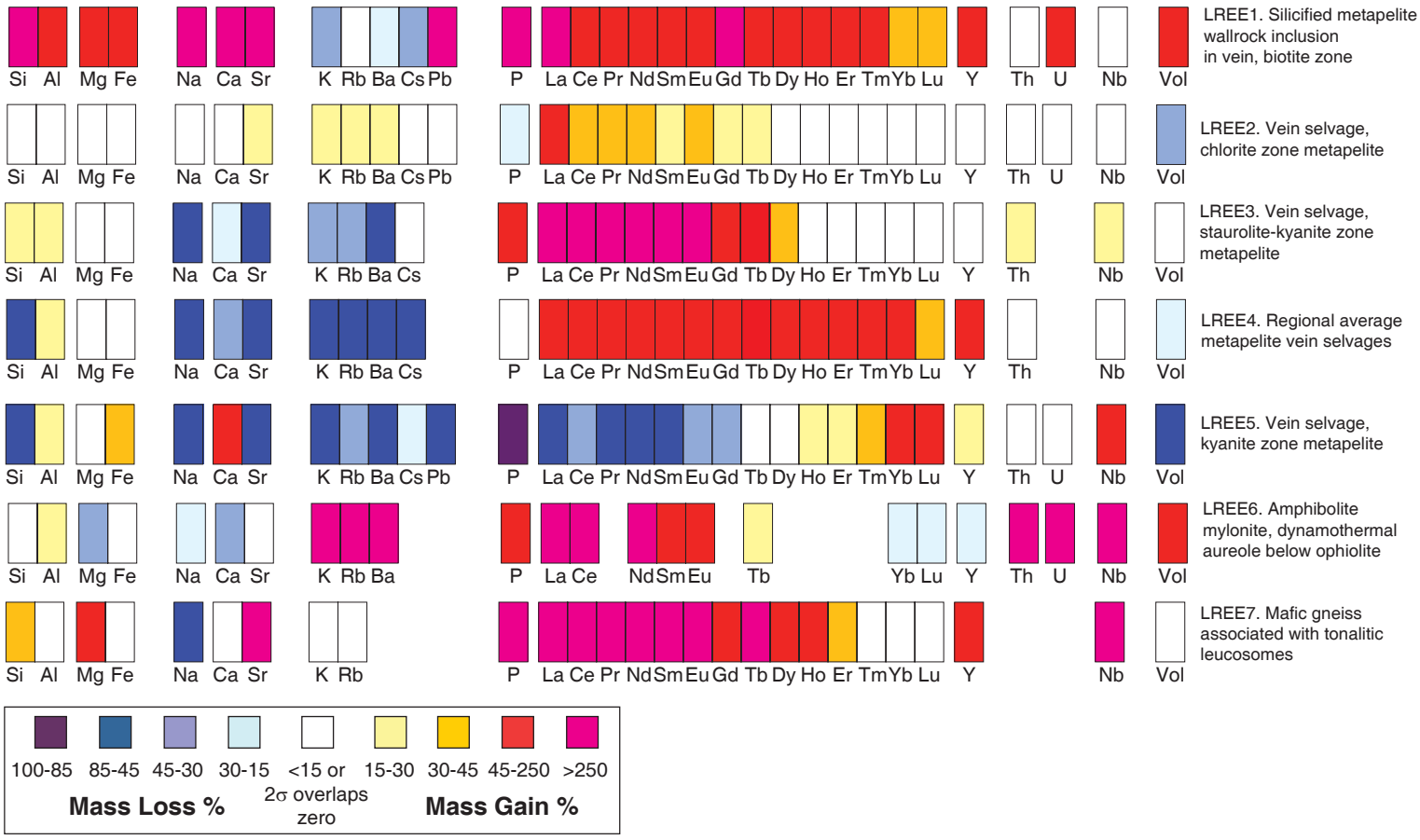

Ague, Fig. 7

This is a preprint, the final version is subject to change, of the American Mineralogist (MSA)
Cite as Authors (Year) Title. American Mineralogist, in press.
(DOI will not work until issue is live.) DOI: http://dx.doi.org/10.2138/am-2017-6130

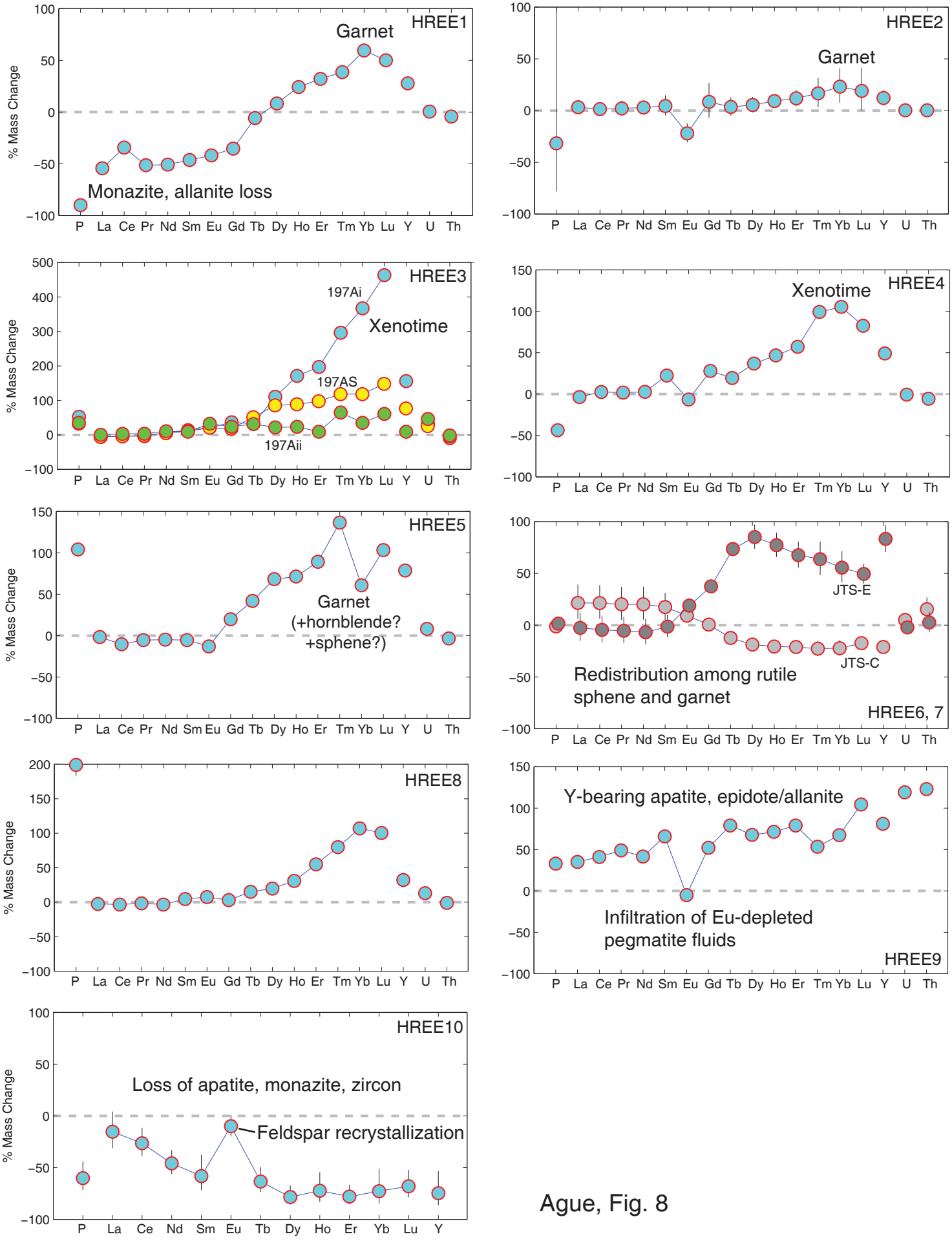

Ague, Fig. 8

This is a preprint, the final version is subject to change, of the American Mineralogist (MSA)
Cite as Authors (Year) Title. American Mineralogist, in press.
(DOI will not work until issue is live.) DOI: http://dx.doi.org/10.2138/am-2017-6130

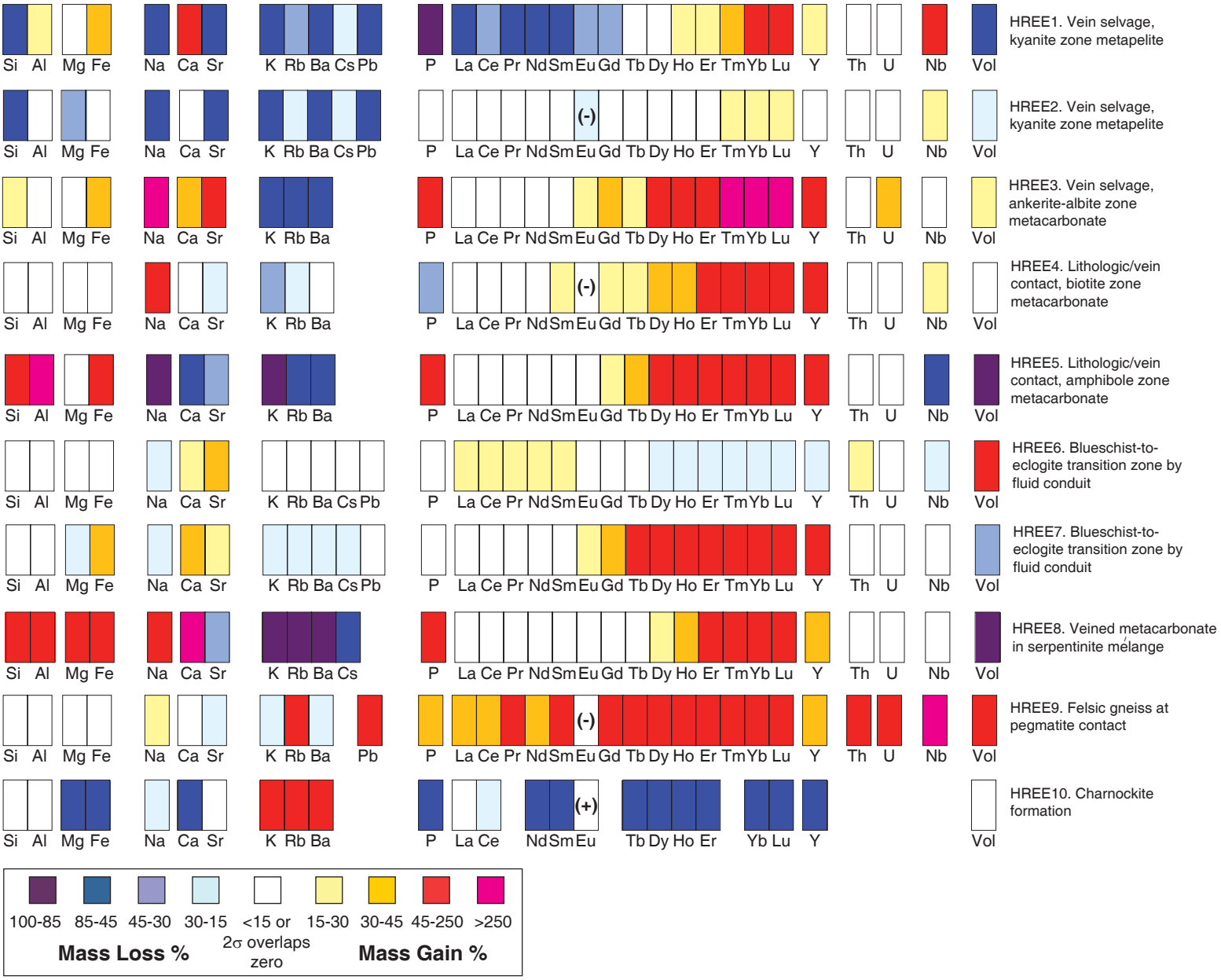

Ague, Fig. 9

This is a preprint, the final version is subject to change, of the American Mineralogist (MSA)
Cite as Authors (Year) Title. American Mineralogist, in press.
(DOI will not work until issue is live.) DOI: http://dx.doi.org/10.2138/am-2017-6130

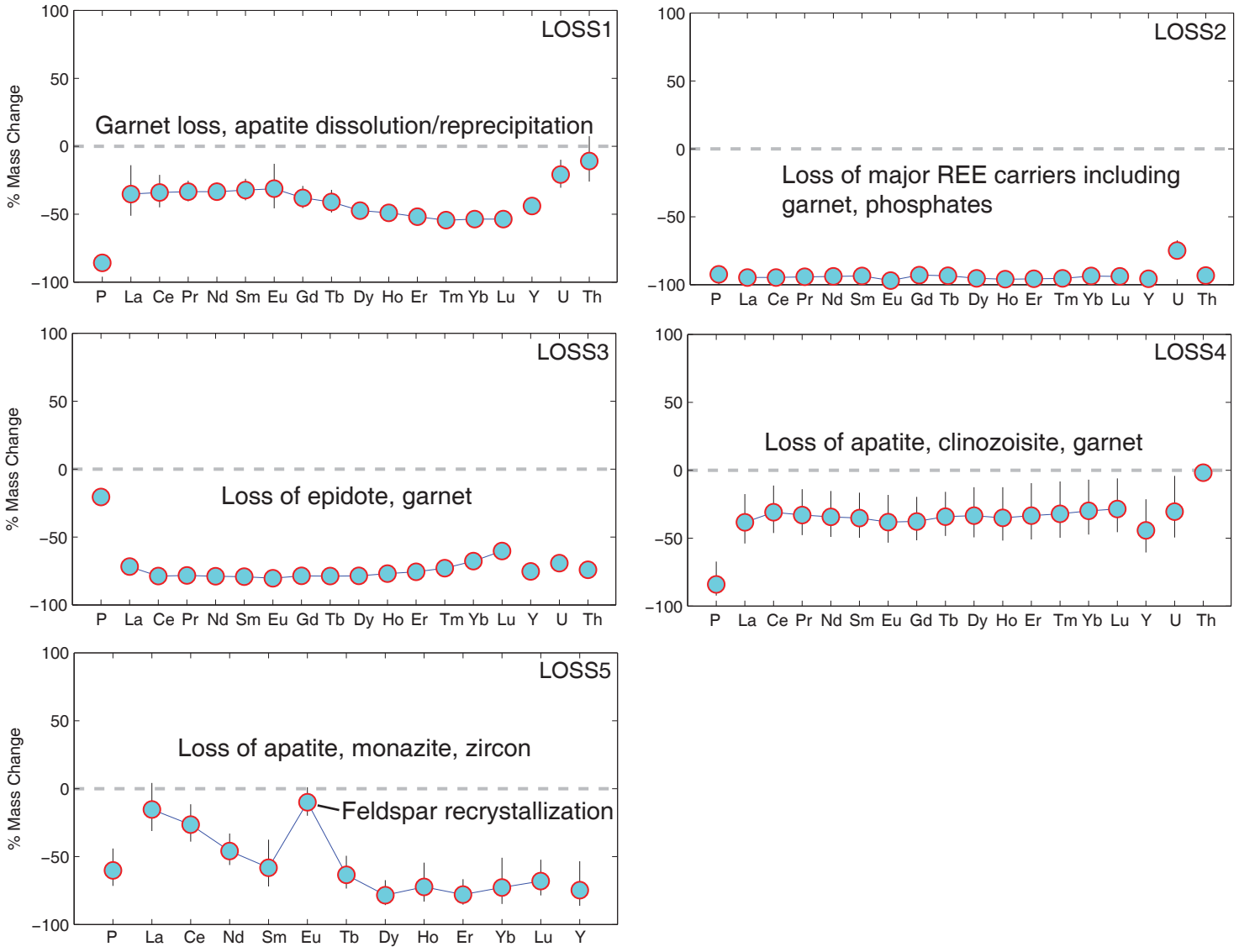

Ague, Fig. 10

This is a preprint, the final version is subject to change, of the American Mineralogist (MSA)
Cite as Authors (Year) Title. American Mineralogist, in press.
(DOI will not work until issue is live.) DOI: http://dx.doi.org/10.2138/am-2017-6130

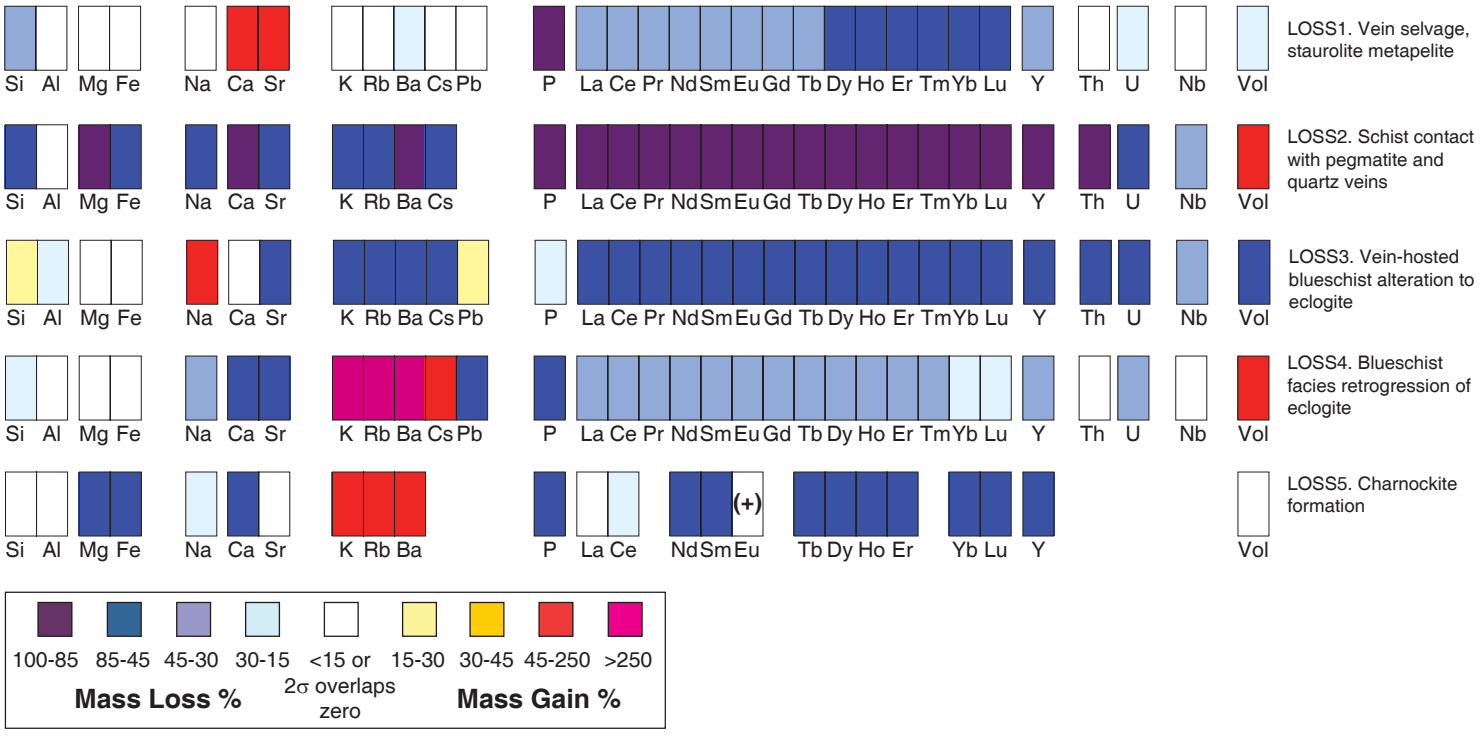

Ague, Fig. 11

This is a preprint, the final version is subject to change, of the American Mineralogist (MSA)
Cite as Authors (Year) Title. American Mineralogist, in press.
(DOI will not work until issue is live.) DOI: http://dx.doi.org/10.2138/am-2017-6130

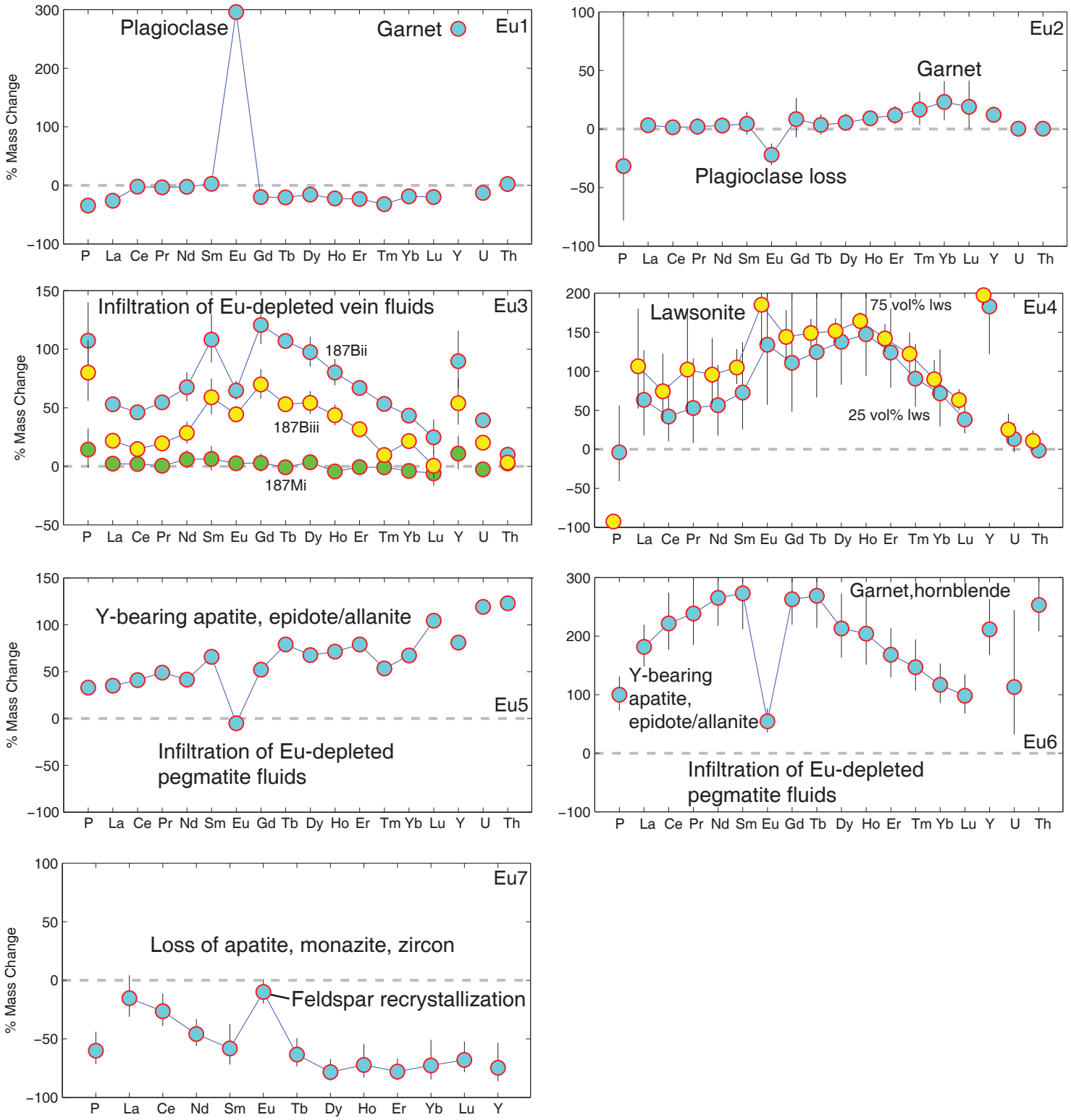

Ague, Fig. 12

This is a preprint, the final version is subject to change, of the American Mineralogist (MSA)
Cite as Authors (Year) Title. American Mineralogist, in press.
(DOI will not work until issue is live.) DOI: http://dx.doi.org/10.2138/am-2017-6130

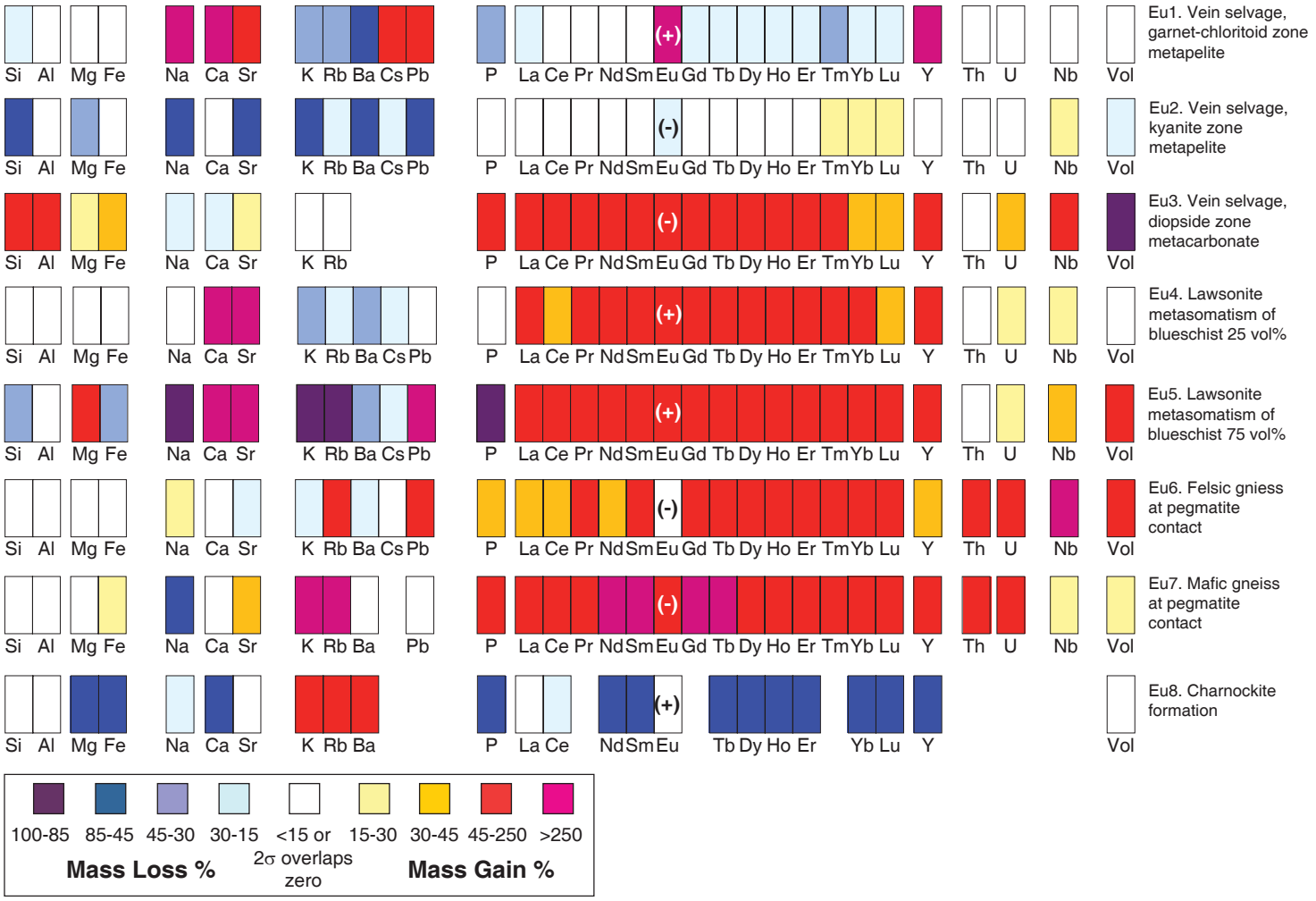

Ague, Fig. 13

This is a preprint, the final version is subject to change, of the American Mineralogist (MSA)
Cite as Authors (Year) Title. American Mineralogist, in press.
(DOI will not work until issue is live.) DOI: http://dx.doi.org/10.2138/am-2017-6130

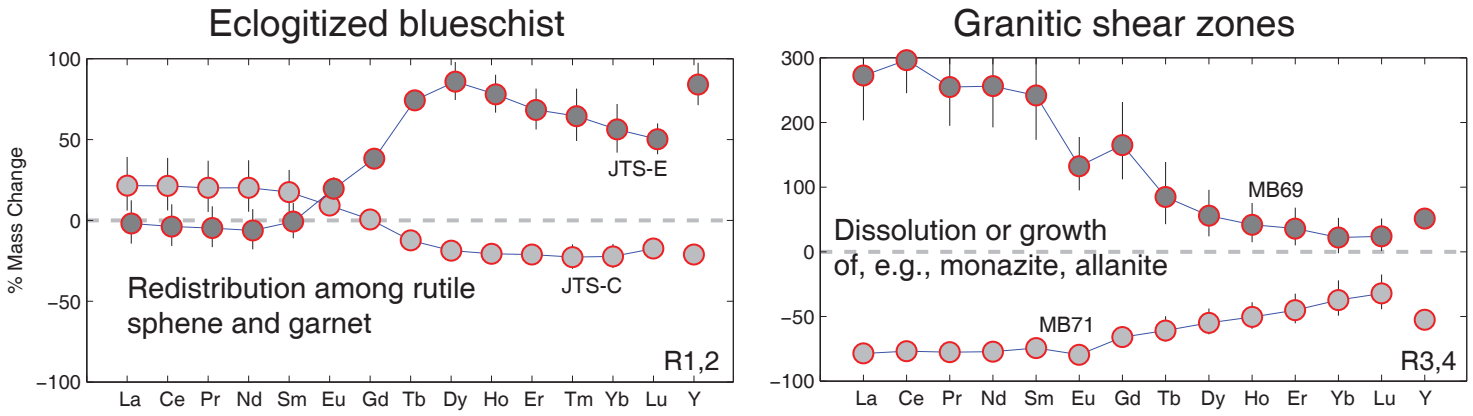

Ague, Fig. 14

This is a preprint, the final version is subject to change, of the American Mineralogist (MSA)
Cite as Authors (Year) Title. American Mineralogist, in press.
(DOI will not work until issue is live.) DOI: http://dx.doi.org/10.2138/am-2017-6130

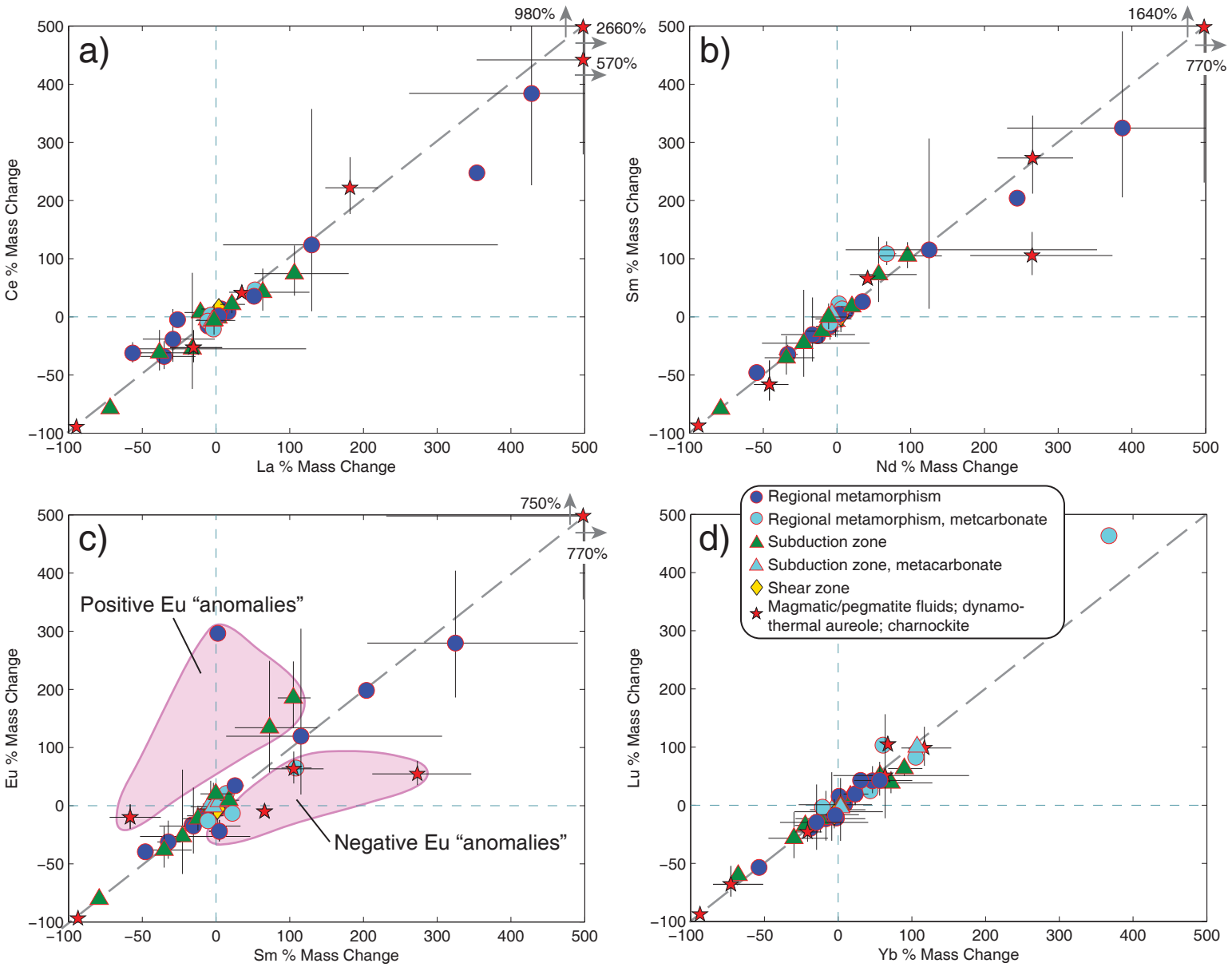

Ague, Fig. 15

This is a preprint, the final version is subject to change, of the American Mineralogist (MSA)
Cite as Authors (Year) Title. American Mineralogist, in press.
(DOI will not work until issue is live.) DOI: http://dx.doi.org/10.2138/am-2017-6130

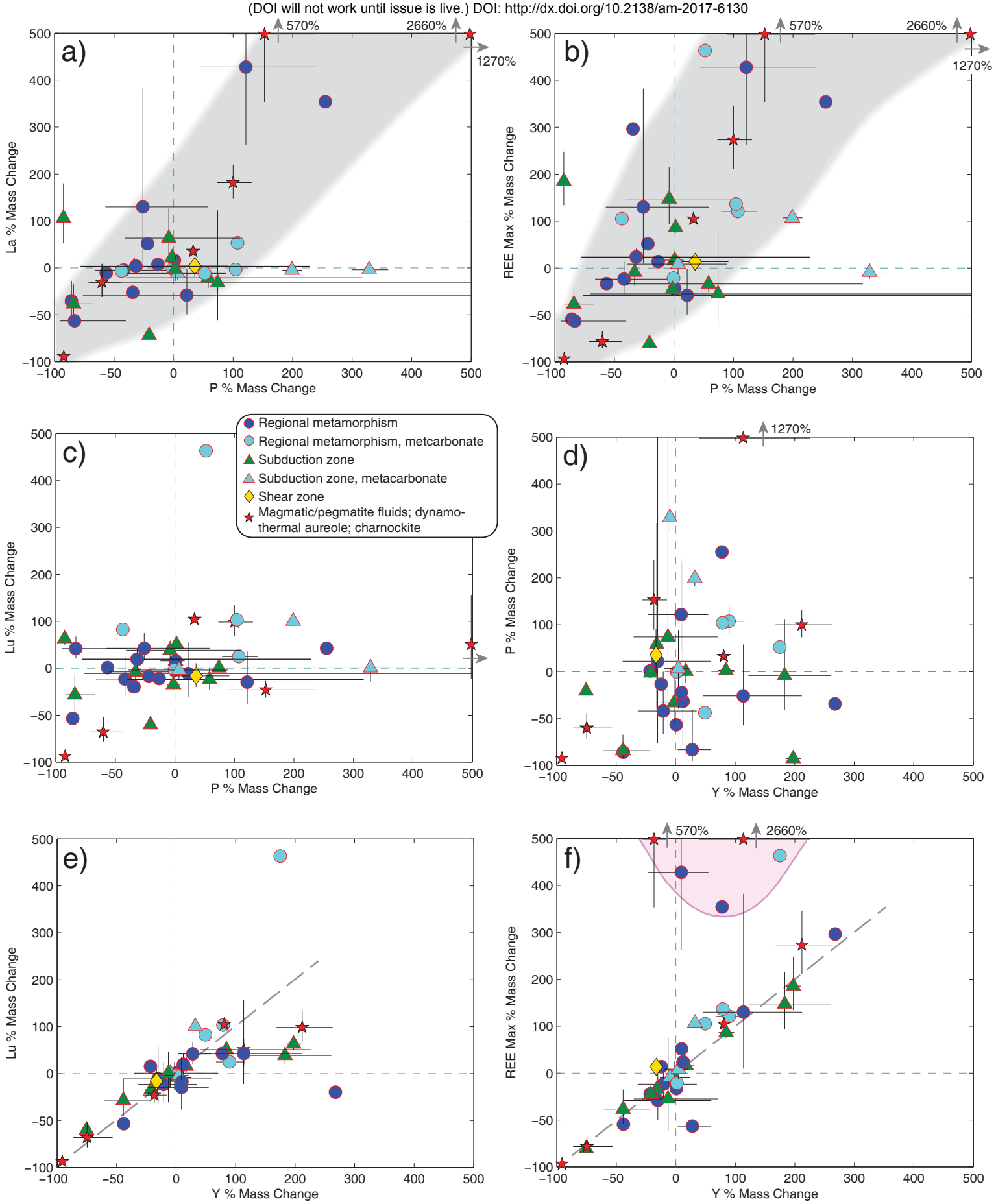

Ague, Fig. 16

This is a preprint, the final version is subject to change, of the American Mineralogist (MSA)
Cite as Authors (Year) Title. American Mineralogist, in press.
(DOI will not work until issue is live.) DOI: http://dx.doi.org/10.2138/am-2017-6130

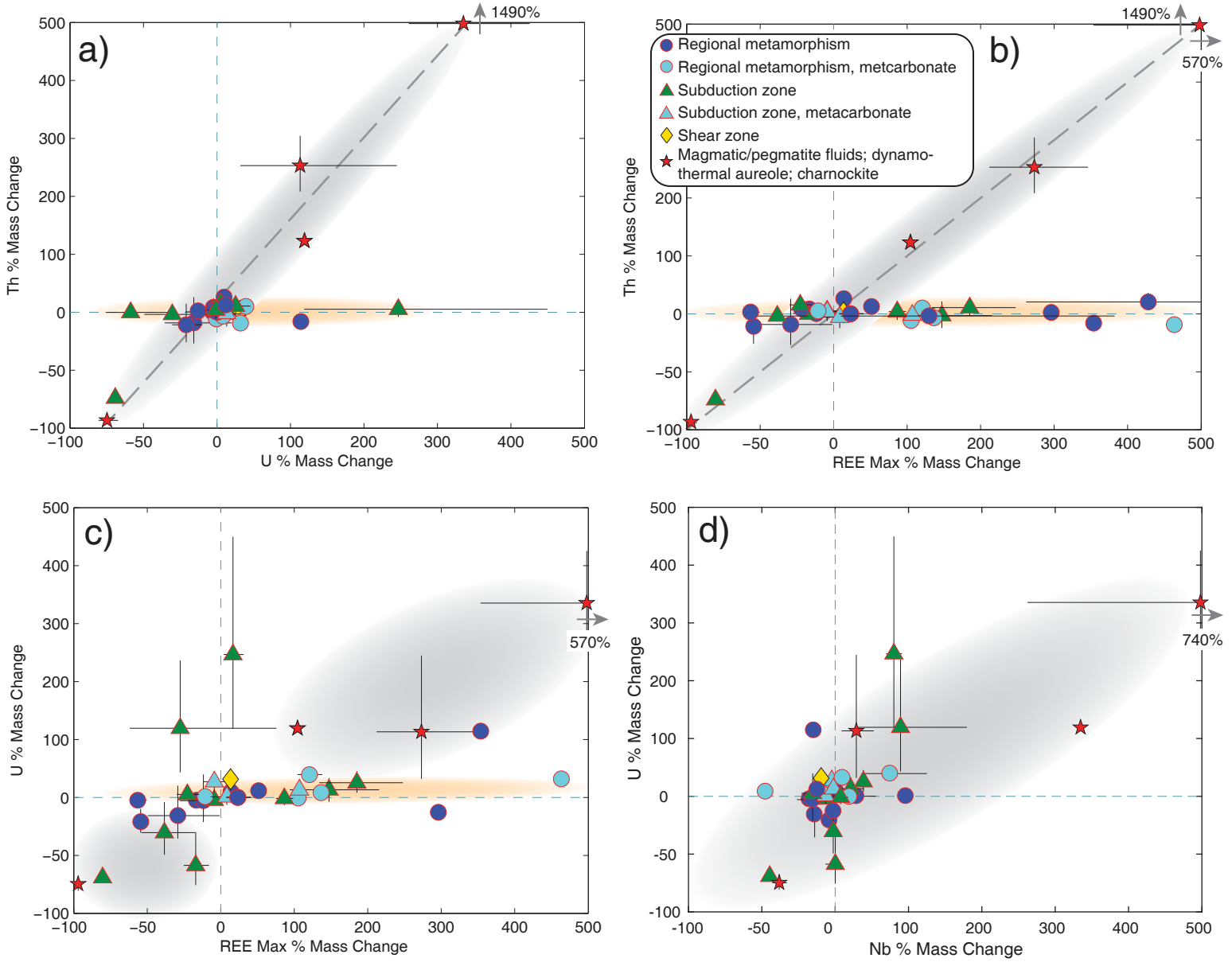

Ague, Fig. 17

This is a preprint, the final version is subject to change, of the American Mineralogist (MSA)
Cite as Authors (Year) Title. American Mineralogist, in press.
(DOI will not work until issue is live.) DOI: http://dx.doi.org/10.2138/am-2017-6130

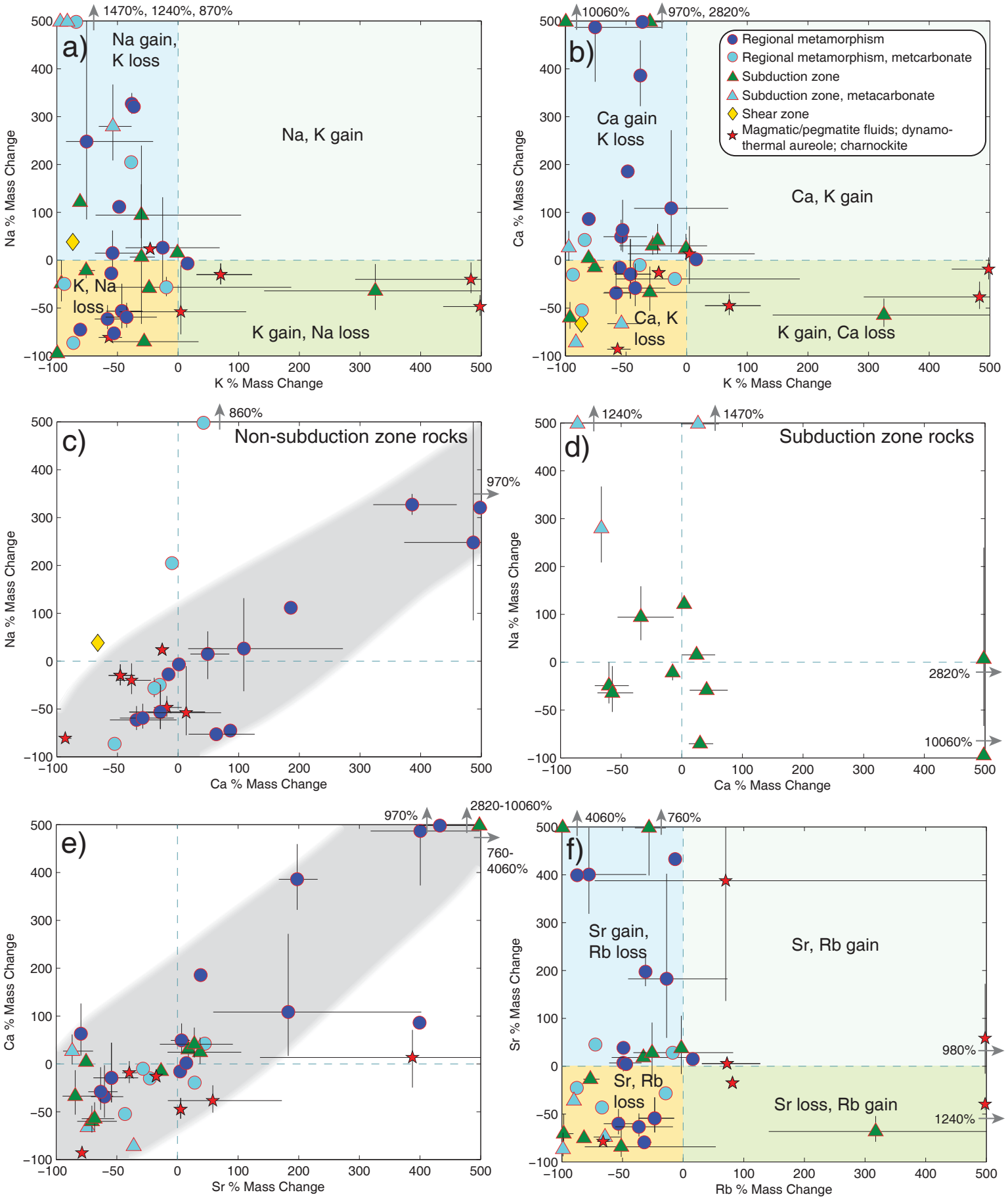

Ague, Fig. 18

This is a preprint, the final version is subject to change, of the American Mineralogist (MSA)
Cite as Authors (Year) Title. American Mineralogist, in press.
(DOI will not work until issue is live.) DOI: http://dx.doi.org/10.2138/am-2017-6130

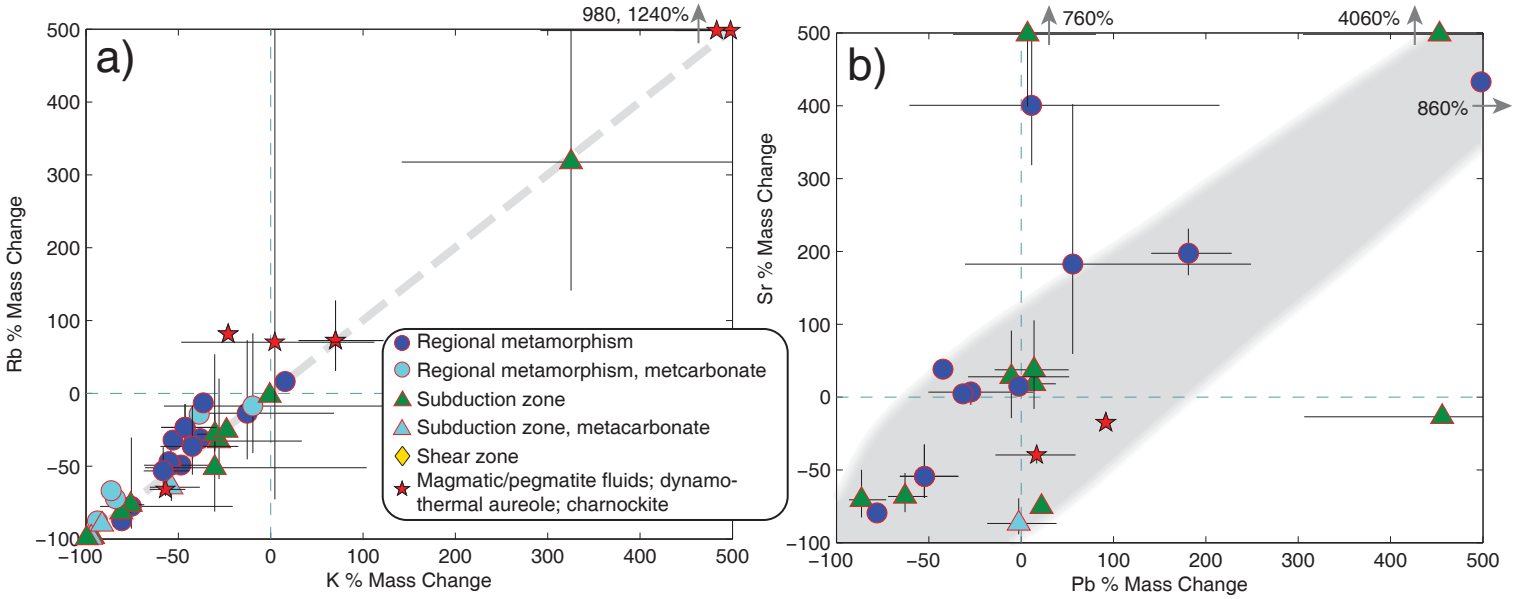

Ague, Fig. 19

This is a preprint, the final version is subject to change, of the American Mineralogist (MSA)
Cite as Authors (Year) Title. American Mineralogist, in press.
(DOI will not work until issue is live.) DOI: http://dx.doi.org/10.2138/am-2017-6130

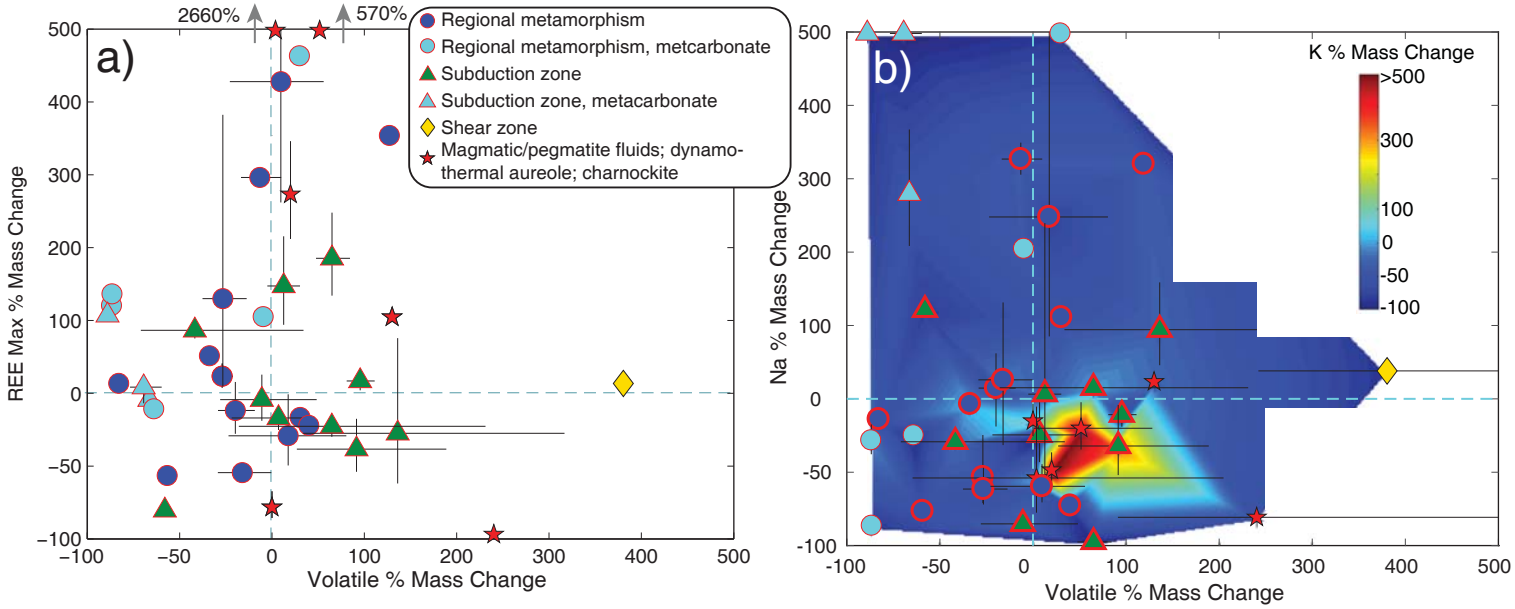

Ague, Fig. 20

This is a preprint, the final version is subject to change, of the American Mineralogist (MSA)
Cite as Authors (Year) Title. American Mineralogist, in press.
(DOI will not work until issue is live.) DOI: http://dx.doi.org/10.2138/am-2017-6130

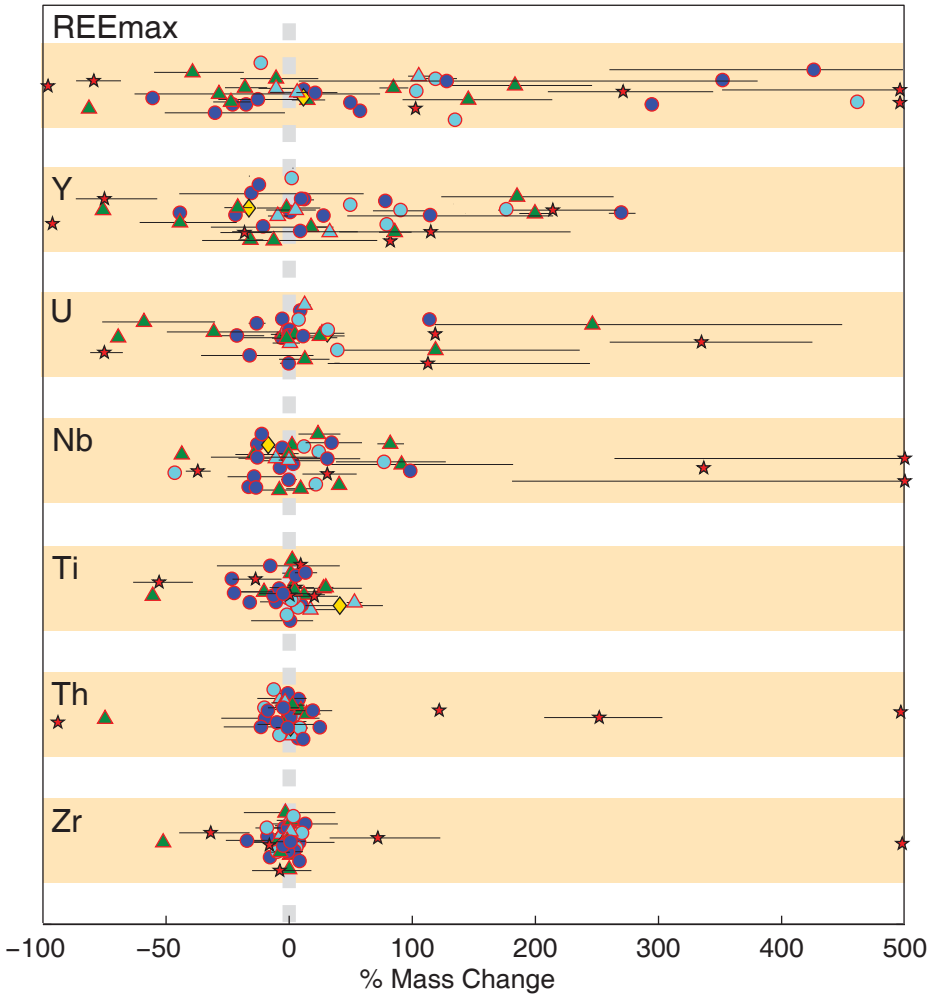

Ague, Fig. 21

This is a preprint, the final version is subject to change, of the American Mineralogist (MSA)
Cite as Authors (Year) Title. American Mineralogist, in press.
(DOI will not work until issue is live.) DOI: http://dx.doi.org/10.2138/am-2017-6130

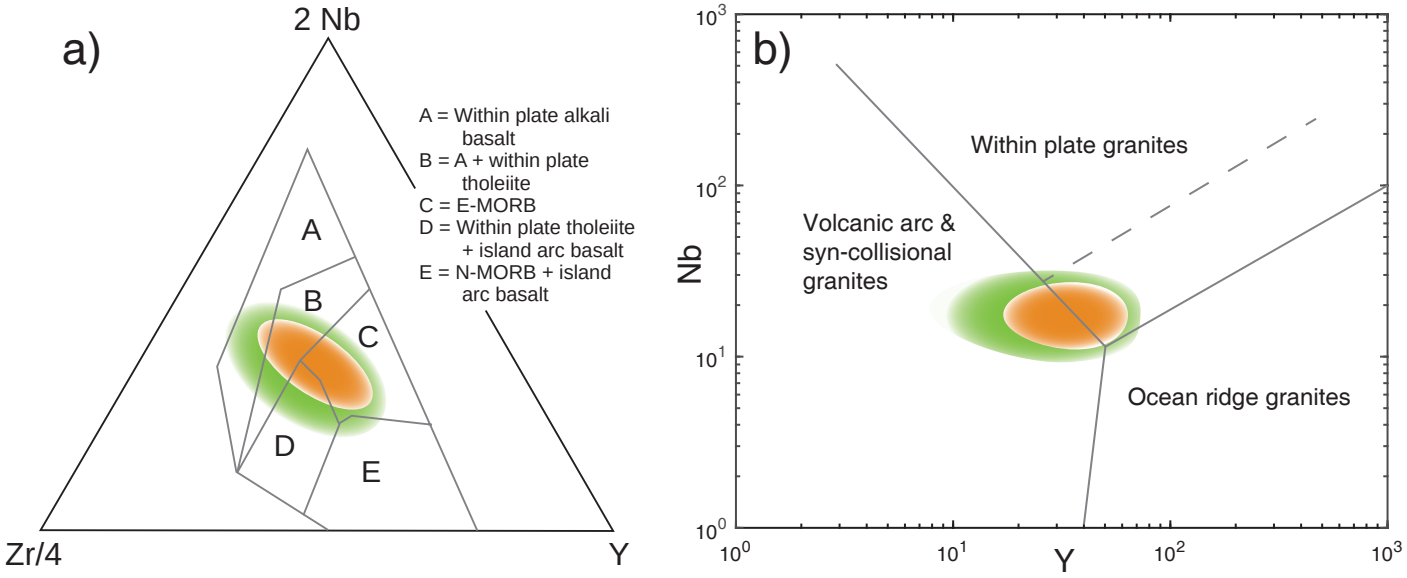

Ague, Fig. 22

This is a preprint, the final version is subject to change, of the American Mineralogist (MSA)
Cite as Authors (Year) Title. American Mineralogist, in press.
(DOI will not work until issue is live.) DOI: http://dx.doi.org/10.2138/am-2017-6130

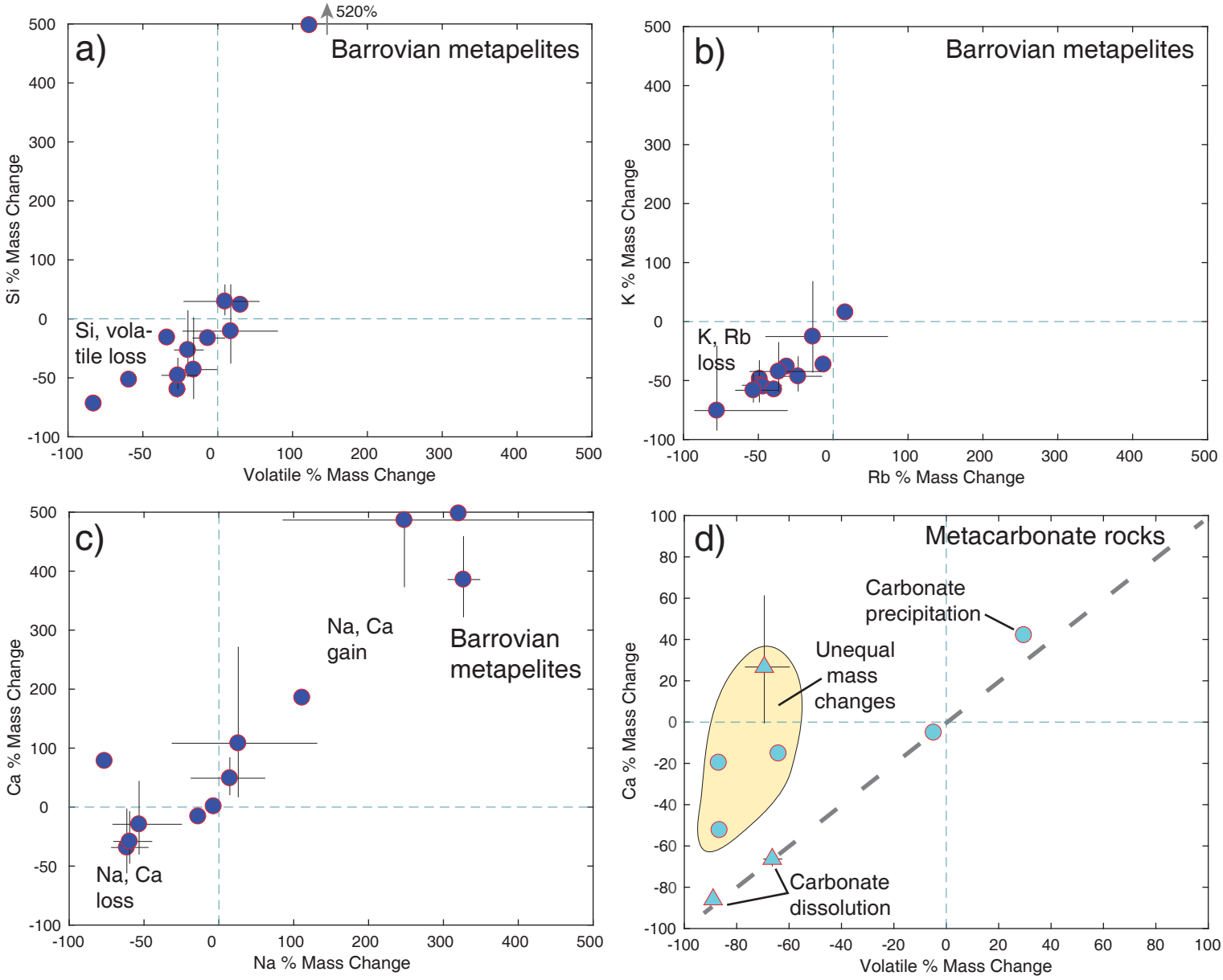

Ague, Fig. 23

This is a preprint, the final version is subject to change, of the American Mineralogist (MSA)
Cite as Authors (Year) Title. American Mineralogist, in press.
(DOI will not work until issue is live.) DOI: http://dx.doi.org/10.2138/am-2017-6130

Table 1. Data sources

Code	Geologic Setting	Rock Category, Notes, and REE_{Max}
	Limited REE Mobility	
LM1	Vein selvage, Barrovian biotite zone metapelite, Scotland.	(1) Masters and Ague (2005) (site 7) and Supplemental Table 1[1]. REE_{Max}=La (-29%)
LM2	Vein selvage, Barrovian garnet-chloritoid zone metapelite, Scotland.	(1) Masters and Ague (2005) (site 1) and Supplemental Table 2. REE_{Max}=Eu (-17%)
LM3	Vein selvages, Barrovian staurolite zone metapelite, Scotland.	(1) Masters and Ague (2005) and (sites 9, 94) and Supplemental Table 3. REE_{Max}=Dy (-12%)
LM4	Vein selvage, kyanite zone metapelite, Waits River Formation, Vermont, USA.	(1) Penniston-Dorland and Ferry (2008), S35-1G samples. REE_{Max}=Ce (14%)
LM5	Epidosite metasomatism of amphibolite, White Rock Formation, Nova Scotia, Canada.	(1) Muecke et al. (1979), Table 1. Average epidosite lens relative to average metabasite. REE_{Max}=Tm (-22%)
LM6	Vein selvage, diopside zone metacarbonate rock, Wepawaug Schist, Connecticut, USA.	(2) Ague (2003), Figure 12F. REE_{Max}=Yb (-11%)
LM7	Metapelitic rock at serpentinite mélange contact, Syros Island, Cyclades, Greece.	(3) Breeding et al. (2004). Altered contact samples E1 and E2 relative to distal samples E3–E5. Site JAGSY-51. REE_{Max}=Ce (-28%)
LM8	Greenschist retrogression of blueschist, Tinos Island, Cyclades, Greece.	(3) Breeding et al. (2002; 2003) and Supplemental Table 4. REE_{Max}=Yb (17%)
LM9	Glaucophanite rind on blueschist-eclogite block in serpentinite mélange, Syros Island, Cyclades, Greece.	(3) Supplemental Table 5. REE_{Max}=Tb (-17%)
LM10	Eclogitized blueschist, Tinos Island, Cyclades, Greece.	(3) Supplemental Table 6. REE_{Max}=Gd (-4%)
LM11	Metacarbonate rock at veined metasedimentary mélange contact, Tinos Island, Cyclades, Greece.	(4) Ague and Nicolescu (2014), Figure S3b. Site JAGTI-18. REE_{Max}=Tm (-4%)
LM12	Metacarbonate rock at serpentinite contact, Malaspina, Corsica, France.	(4) Galvez et al. (2013), Figure 6. REE_{Max}=Tb (8%)
LM13	Greenschist facies shear zones cutting granitic rocks, Mont Blanc Massif, Western Alps.	(5) Rolland et al. (2003). Sample C33. REE_{Max}=Ce (13%)
	LREE Mobility	
LREE1	Silicified metapelite wallrock inclusions in vein, Barrovian biotite zone, Scotland.	(1) Masters and Ague (2005) (site 82) and Supplemental Table 7. 82 II 1D used for main data set herein. Mass transfer for 82 II 1E also shown in Figure 6. REE_{Max}=La (350%)
LREE2	Vein selvage, chlorite zone metapelite, Waits	(1) Penniston-Dorland and Ferry (2008). S40-

[1]Deposit item AM-xyz, Supplemental Tables. Deposit items are stored on the MSA web site and available via the American Mineralogist Table of Contents. Find the article in the table of contents at GSW (ammin.geoscienceworld.org) or MSA (www.minsocam.org), and then click on the deposit link.

	River Formation, Vermont, USA.	1D samples. REE_{Max}=La (51%)
LREE3	Vein selvage, staurolite-kyanite zone, Unst, Shetland Islands, Scotland.	(1) Bucholz and Ague (2010) (site 181). 181Aiii selvage relative to less altered samples 181B, C, D, and E used in main data set herein. 181Aii selvage relations also shown in Figure 6. REE_{Max}=La (430%)
LREE4	Regional vein selvage average, Unst, Shetland Islands, Scotland.	(1) Bucholz and Ague (2010), Figure 6. REE_{Max}=La (130%)
LREE5& HREE1	Vein selvage, kyanite zone metapelite, Wepawaug Schist, Connecticut, USA.	(1) Ague (2011). Sample JAW-114i selvage margin relative to most distal sample 114vi. REE_{Max}=Yb (59%); Pr loss has comparable absolute value (-51%)
LREE6	Biotite amphibolite, mylonite shear zone in dynamothermal aureole below an ophiolite remnant.	(6) Dostal et al. (1980). Epidote and quartz amphibolite used as precursors. REE_{Max}=La (570%)
LREE7	Clino- and orthopyroxene reaction zones, margins of mafic gneiss lenses/layers associated with tonalitic leucosomes.	(6) Pan and Fleet (1996). REE_{Max}=La (2660%)
LREE8 & R3	Shear zones cutting granitic rocks, Mont Blanc Massif, Western Alps.	(5) Rolland et al. (2003). Sample MB69. REE_{Max}=Ce (300%)
LREE9 & R4	Shear zones cutting granitic rocks, Mont Blanc Massif, Western Alps.	(5) Rolland et al. (2003). Sample MB71. REE_{Max}=Eu (-81%)

HREE Mobility

HREE1	Vein selvage, kyanite zone metapelite, Wepawaug Schist, Connecticut, USA.	(1) Ague (2011). Sample JAW-114i selvage margin relative to most distal sample 114vi. REE_{Max}=Yb (59%); Pr loss has comparable absolute value (-51%)
HREE2	Average vein selvage, kyanite zone metapelite, Wepawaug Schist, Connecticut, USA.	(1) Ague (2011). Site JAW-165A, south profile. REE_{Max}=Yb (23%)
HREE3	Vein selvage, metacarbonate rock, metacarbonate ankerite-albite zone, Wepwaug Schist, Connecticut, USA	(2) Ague (2003), Figure 6A. JAW-197Ai selvage relations used for main data set herein. Selvage mass transfer for samples 197AS and 197Aii also shown in Figure 8. REE_{Max}=Lu (460%)
HREE4	Metacarbonate rock at contact with metapelite, metacarbonate biotite zone, Wepawaug Schist, Connecticut, USA.	(2) Ague (2003), Figure 8A. JAW-171A. REE_{Max}=Yb (105%)
HREE5	Metacarbonate rock at veined lithologic contact, metacarbonate amphibole zone, Wepawaug Schist, Connecticut, USA.	(2) Ague (2003), Figure 10C. JAW-181Rii. REE_{Max}=Tm (140%)
HREE6	Eclogitized blueschist adjacent to fluid conduit, Tian Shan, China.	(3) Beinlich et al. (2010). Blueschist-eclogite transition zone sample C relative to blueschist hosts A and B. REE_{Max}=Tm (-23%)
HREE7	Eclogitized blueschist adjacent to fluid	(3) Beinlich et al. (2010). Blueschist-eclogite transition zone sample E relative to blueschist

	conduit, Tian Shan, China.	hosts A and B. REE_{Max}=Dy (86%)
HREE8	Veined metacarbonate rock in contact with serpentinite mélange, Syros Island, Cyclades, Greece.	(4) Ague and Nicolescu (2014), Figure S3a. Site JAGSY-37. REE_{Max}=Yb (110%)
HREE9	Felsic gneiss at pegmatite contact, Napier Complex, East Antarctica.	(6) Carson and Ague (2008), Figure 6a. Series 28. REE_{Max}=Lu (105%)
HREE10, Eu8, & LOSS5	Charnockite formation, incipient granulite facies, Kabbaldurga, India.	(6) Stähle et al. (1987), Table 2. Chanockite and pegmatitic charnockite relative to gneiss. REE_{Max}=Dy (-78%)

Loss of REE

LOSS1	Vein selvage, Barrovian staurolite zone, Scotland.	(1) Masters and Ague (2005) (site 109) and Supplemental Table 8. REE_{Max}=Tm (-54%)
LOSS2	Sillimanite schist in contact with pegmatite and quartz veins.	(6) Supplemental Table 9. REE_{Max}=Eu (-97%)
LOSS3	Vein-hosted eclogite facies blueschist alteration zone in blueschist host, Tian Shan, China.	(3) John et al. (2008), Figure 11. REE_{Max}=Eu (-80%)
LOSS4	Phengite-ankerite blueschist rehydration of eclogite, Tian Shan, China.	(3) van der Straaten et al. (2008). REE_{Max}=La (-38%)
LOSS5, Eu8 & HREE10	Charnockite formation, incipient granulite facies, Kabbaldurga, India.	(6) Stähle et al. (1987), Table 2. Chanockite and pegmatitic charnockite relative to gneiss. REE_{Max}=Dy (-78%)

Eu "Anomalies"

Eu1	Vein selvage, Barrovian garnet-chloritoid zone metapelite, Scotland.	(1) Ague (1997) (site 101L), Masters and Ague (2005), and Supplemental Table 10. REE_{Max}=Eu (300%)
Eu2 & HREE2	Average vein selvage, kyanite zone metapelite, Wepawaug Schist, Connecticut, USA.	(1) Ague (2011). Site JAW-165A, south profile. REE_{Max}=Yb (23%)
Eu3	Metacarbonate rock at veined lithologic contact, diopside zone, Wepawaug Schist, Connecticut, USA.	(2) Ague (2003), Figures 17A, B. JAW-187Bii altered zone used in main data set herein. Geochemical relations for selvage sample 187Biii and distal sample 187Mi also shown in Figure 12. REE_{Max}=Gd (120%)
Eu4	Lawsonite metasomatism in blueschist facies metapelites at contacts with serpentinite, Schistes Lustrés complex, Corsica, France.	(3) Vitale Brovarone et al. (2013), Table 1; 25 vol% lawsonite. REE_{Max}=Ho (150%)
Eu5	Lawsonite metasomatism in metapelites at contacts with serpentinite, Schistes Lustrés complex, Corsica, France.	(3) Vitale Brovarone et al. (2013), Table 1; 75 vol% lawsonite. REE_{Max}=Eu (185%)
Eu6 & HREE9	Felsic gneiss at pegmatite contact, Napier Complex, East Antarctica.	(6) Carson and Ague (2008), Figure 6a. Series 28. REE_{Max}=Lu (105%)
Eu7	Mafic gneiss at pegmatite contact, Napier	(6) Carson and Ague (2008), Figure 7. Series

	Complex, East Antarctica.	76. Contact sample 76/1B relative to distal samples 76/7B– 76/9B. REE_{Max}=Sm (270%)
Eu8, LOSS5,& HREE10	Charnockite formation, incipient granulite facies, Kabbaldurga, India.	(6) Stähle et al. (1987), Table 2. Chanockite and pegmatitic charnockite relative to gneiss. REE_{Max}=Dy (-78%)
	Redistribution of REE	
R1 & HREE6	Eclogitized blueschist adjacent to fluid conduit, Tian Shan, China.	(3) Beinlich et al. (2010). Blueschist-eclogite transition zone sample C relative to blueschist hosts A and B. REE_{Max}=Tm (-23%)
R2 & HREE7	Eclogitized blueschist adjacent to fluid conduit, Tian Shan, China.	(3) Beinlich et al. (2010). Blueschist-eclogite transition zone sample E relative to blueschist hosts A and B. REE_{Max}=Dy (86%)
R3 & LREE8	Greenschist facies shear zones cutting granitic rocks, Mont Blanc Massif, Western Alps.	(5) Rolland et al. (2003). Sample MB69. REE_{Max}=Ce (300%)
R4 & LREE9	Greenschist facies shear zones cutting granitic rocks, Mont Blanc Massif, Western Alps.	(5) Rolland et al. (2003). Sample MB71. REE_{Max}=Eu (-81%)

Notes: Rock Categories: (1) regional metamorphism (non-subduction); (2) regional metamorphism, metacarbonate rocks (non-subduction) ; (3) subduction zone; (4) subduction zone metacarbonate rocks ; (5) shear zones, granitic rocks; (6) dynamothermal aureole (shear zone), magmatic/pegmatite fluid infiltration, charnockite. Percentage mass change for REE_{Max} element given in parentheses.